Mariana Lourenço Palma Campaniço

Licenciatura em Bioquímica

Electrochemical characterisation of Formate dehydrogenase and its catalytic properties

Dissertação para obtenção do Grau de Mestre em

Biotecnologia

Orientador: Cristina M. Cordas, Investigadora Pós-Doutoramento, LAQV, REQUIMTE, FCT-UNL

Co-orientador: Luísa B. Maia, Investigadora Pós-Doutoramento, LAQV, REQUIMTE, FCT-UNL

Co-orientador: Professor José J. G. Moura, Professor Catedrático (Aposentado), LAQV, REQUIMTE, FCT-UNL

Presidente: Prof. Doutora Susana Barreiros, FCT-UNL

Arguente(s): Prof. Doutor Luís Joaquim Pina da Fonseca, IST-UL

Vogal(ais): Doutora Cristina M. Cordas, FCT-UNL

FACULDADE DE CIÊNCIAS E TECNOLOGIA
UNIVERSIDADE NOVA DE LISBOA

Electrochemical characterisation of Formate dehydrogenase and its catalytic properties

Agradecimentos

Aqui deixo o meu agradecimento a todos os que contribuíram para a realização desta tese e para a minha aprendizagem e evolução como cientista.

Ao Professor José J. G. Moura, por me ter dado esta oportunidade de realizar esta tese e de me receber tão bem no seu laboratório.

À Doutora Cristina M. Cordas, por toda a paciência e disponibilidade que teve durante todas as fases desta tese. Obrigada pela confiança que teve em mim e por todo o conhecimento em eletroquímica que me transmitiu.

À Doutora Luísa B. Maia, por toda a ajuda, disponibilidade e boa disposição durante a grande aventura que foi o processo de purificação.

À Rita Batista, por toda a sua ajuda e pela sua paciência comigo (mesmo quando eu tinha fome).

A todas a pessoas do grupo do Biological Chemistry pela amizade, profissionalismo e constante disponibilidade para qualquer dúvida que eu tivesse.

Às minhas colegas de casa, Carolina e Raquel, por toda a paciência e pela preocupação de certificarem que estava tudo bem comigo.

Aos meus amigos, Vânia Silva, Patrícia Freitas, Hugo Miguel, Tatiana Guerreiro que estiveram sempre a meu lado, sempre disponíveis tanto para apoio como para brincadeira.

À minha família, que apesar de estar longe, esteve sempre comigo. Por sempre me apoiarem e acreditarem em mim mesmo quando eu não acreditava em mim própria.

Resumo

Nos últimos anos, a quantidade de CO_2 libertada para a atmosfera do planeta tem aumentado exponencialmente devido à dependência global de combustíveis fósseis. Este é um dos principais responsáveis para as alterações climáticas observadas atualmente. Por outro lado, devido à abundância de CO_2, há um interesse crescente no desenvolvimento de estratégias para utilizar o CO_2 na produção de compostos de valor acrescentado com interesse para industrias das energias "verdes" e da síntese química sustentável.

As formato desidrogenases (FDH) são uma classe de enzimas que catalisam a interconversão reversível do formato em CO_2. Estas enzimas apresentam diferentes composições em termos de subunidades e podem conter um átomo de molibdénio ou tungsténio no centro ativo.

Até à data, a caracterização eletroquímica destas proteínas nunca tinha sido feita usando métodos diretos, não mediados. Nesta Tese, a purificação da FDH de *Desulfovibrio desulfuricans* e a sua caracterização eletroquímica não mediada foi conseguida pela primeira vez. O comportamento eletroquímico do centro catalítico da enzima foi observado usando métodos eletroquímicos diretos, nomeadamente voltametria cíclica, tendo sido possível determinar parâmetros termodinâmicos e cinéticos, tais como o seu potencial formal ($E^{0'}$ = -245 $\pm$ 8 mV vs NHE) e a constante heterogénea de transferência electrónica. Foi também possível observar a atividade catalítica da FDH para a redução do CO_2 por técnicas eletroquímicas diretas.

Palavras Chave: Formato desidrogenase; Bioelectroquímica; Catálise enzimática; Redução de CO_2;

Abstract

In recent years the amount of CO_2 release into the planet atmosphere has increase exponentially due to a global dependency in fossil fuels. This is one of the major contributors to the climate change that is seen nowadays. On the other hand, due to the CO_2 abundance, there has been an interest in developing methods to harvest and use this CO_2 in the production of green energy and sustainable chemistry.

Formate dehydrogenase (FDH) proteins are a class of metalloenzymes with different subunit composition containing either molybdenum or tungsten at the active site. FDH catalyses the oxidation of formate into CO_2. Recently it was shown that some of the FDH enzymes have the ability to perform the reverse reaction that is, these can catalyse the reversible interconversion of CO_2 and formate.

However, to date, the electrochemical characterisation of the protein has not yet been attained using direct, non-mediated methods. In this thesis the isolation of FDH from *Desulfovibrio desulfuricans,* its biochemical and non-mediated electrochemical characterisation was attained. The redox features of the Mo catalytic centre of the enzyme, including thermodynamic and kinetic parameters such as its formal reduction potential ($E^{0'}$ = -245 $\pm$ 8 mV vs NHE) and heterogeneous electron transfer constant, were determined, for the first time, using direct electrochemical methods. The catalytic activity towards the CO_2 reduction was also observed, for the first time, by direct electrochemical techniques.

Keywords: Formate dehydrogenase; Bioelectrochemistry; Enzymatic catalysis, CO_2 Reduction;

Abbreviations, Symbols and Constants

Abbreviations

BV – Benzyl Viologen

Cys – Cysteine

D. desulfuricans - Desulfovibrio desulfuricans

FDH - Formate dehydrogenase

Fe/S centre – Iron-Sulfur centre

MV – Methyl Viologen

Native-PAGE - Polyacrylamide gel electrophoresis under native conditions

SDS - PAGE - Polyacrylamide gel electrophoresis, under denaturating conditions, in the presence of sodium dodecyl sulfate,

SDS - Sodium Dodecyl Sulfate

SeCys - Selenocyteine

Symbols and Constants

A - Ampere

[O] - Concentration of oxidised species

C - Coulomb

ε - Molar extinction coefficient

$\varnothing$ - Diameter

E - Potential

$E^{0'}$ - Formal reduction potential

E_{p} - Peak potential

E_{pa} - Anodic peak potential

E_{pc} - Cathodic peak potential

ΔE_p - Difference between the anodic and cathodic peak potentials

F - Faraday constant

h – height

I - Current

I_p - Maximum peak current

I_{pa} - Maximum anodic peak current

I_{pc} - Maximum cathodic peak current

k_{sh} - Heterogeneous electron transfer rate constant

m - number of mol

nA - Nanounits of absorbance

n - Number of electrons

Q - Total Electric Charge

R - Molar gas constant

SD – Standard Deviation

T - Temperature

v - Scan rate

V - Volt

Table of Content

Figure Index

Tables Index

1. Introduction

1.1 The problem: global warming and the CO_2 levels

Over the last century, our planet has experienced an unparalleled growth in energy consumption, which has been fuelled by both population increase and technology advances. To meet this demand, the world has developed a high dependence on fossil fuels, like petroleum, natural gas or coal. These resources give us a constant high-quality energy at low cost financially, but, through their use, many toxic compounds are released to our environment, including nitrogen oxides, sulphur oxides, heavy metals and several volatile organic compounds, including CO_2.[1]

On the surface, CO_2 appears harmless. It is non-toxic to humans; it occurs naturally and provides a primary source of carbon for photosynthesis in plants and some microorganisms. However, CO_2 is also a greenhouse-effect gas and its rise has been linked with the average global temperature of the planet, as seen in figure 1.1.[2,3] According to the current statistics, the CO_2 levels will increase up to 800 ppm during this century, which will lead to an increase in ocean acidification and severe global climate changes. [4,5]

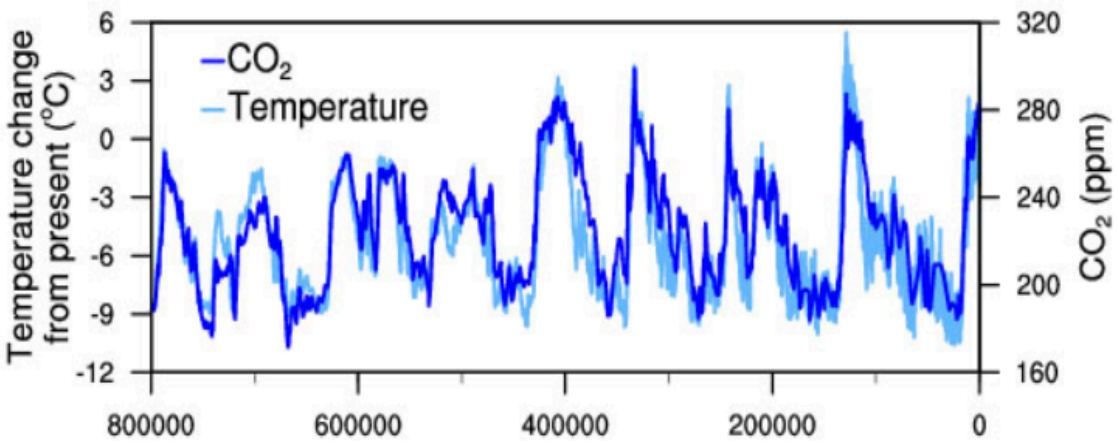

Figure 1.1 Evolution of temperature (light blue) and CO_2 concentration (dark blue) in ice cores in Antarctica. [58]

As a result of the large amounts of CO_2 present in the atmosphere, there has been an interest in developing strategies to harvest and reduce CO_2, not only to mitigate the CO_2 pernicious effects, but also to make use of CO_2 to produce carbon-based compounds that later can be converted into "greener" fuels and value-added chemicals. [6,7] The conversion of CO_2 in formate is one interesting approach to achieve this. The conversion of CO_2 into formate is one interesting approach to achieve this, since formate is more easily transported, handled and stored than other alternative feedstocks. In addition, formate is also the first stable intermediate in the CO_2 -dependent methane production. Secondly, formate is the first stable intermediate during the reduction of CO_2 towards methane. Formate is more easily transported, handled and stored than other alternatives like hydrogen.[8,9]

However, CO_2 is a thermodynamically and kinetically very stable molecule, making its activation a very difficult task. Nevertheless, its direct electrochemical reduction can be achieved if a high overpotential is applied. However, an unwanted variety of products is formed, making the direct electrochemical approach a poor option to handle CO_2. Nature, on the contrary, has developed several different strategies to "easily" activate CO_2., at very mild conditions. So, using a *specific* enzyme as a catalyst for the CO_2 reduction is a very promising approach to attain the *specific* reduction of CO_2 to a *specific* product.[10]

In this Thesis, the use of a Formate dehydrogenase (FDHs) enzyme was explored, aiming to develop a new efficient biocatalysts for the atmospheric CO_2 conversion into formate. In order to overcome this problem, enzymes have been used as catalysts.

1.2 Formate dehydrogenases

Formate dehydrogenases (FDHs) are a group of enzymes that can be found in both prokaryotes and eukaryotes. They participate in a diverse number of biochemical pathways, including biosynthetic pathways and energy metabolism, in different cellular locations, and, therefore they use different physiological redox partners (cytochromes, ferredoxins, NADH/NAD^+ or membrane quinols)[11,12] In order to fulfil each pathway and each respective function, FDHs have evolved into a diverse group of proteins, that contain/harbour various redox centres, like haems or iron-sulfur centres (Fe/S centre), or no centres at all, and displaying different subunits compositions and quaternary structures. [13]

FDH catalyse the reversible two-electron oxidation of formate into CO_2, according Eq. 1. [13] The low reduction potential value of this reaction ($E^{0'}$ = -0.43V) allows prokaryotes to use the formate oxidation to derive energy when the microorganism is under stress conditions, such as anoxic environments. Under these conditions, formate, produced from pyruvate during the anaerobic respiration, serves as a major electron donor to a large variety of respiratory pathways

that use terminal acceptors other than dioxygen.[14–16] During the 1970s, it was reported that some FDHs were also capable of performing the opposite reaction, the reduction of CO_2.[17–19] This reaction can occur both *in vivo* or *in vitro,* provided that they are given the appropriate conditions. [13]

$$HCOO^- \rightleftharpoons CO_2 + 2e^- + H^+ \qquad E^{0'} = -0.43V \qquad \text{(Eq.1)}$$

FDHs can be divided into two different classes, based on the constitution of the active site and, consequently, on their catalytic strategies. One class, the metal-independent FDH class, comprises enzymes that are NAD^+-dependent and have no metal ions or other redox centres. These are the most common and can be found in aerobic bacteria, yeasts, fungi and plants. It is suggested that the catalysis in this FDH class involves the direct hydride transfer from formate to NAD^+.[20,21] The other class is the metal-dependent FDHs. These enzymes are present/found only in prokaryotic organisms and their active site contains one molybdenum or one tungsten ion that mediates the formate formation. [11,12]

1.2.1 Structure

Metal-dependent FDH can have a structural organization very diverse, in order to accomplish the respective function that each pathway requires. There are FDHs that need to be connected to the membrane in order to interact with the membrane-associated electron acceptors. [22] Other FDHs, that are cytoplasmic or periplasmic, have their own electron acceptors like cytochromes, ferredoxins or NAD^+. The crystal structures of three of these enzymes have been reported. Two of them are molybdenum-containing enzymes, FDH-H (figure 1.2 B) and the membrane bound FDH-N, both *E. coli*; the third one is the tungsten-containing FDH from *Desulfovibrio gigas* (Figure 1.2 A).[13]

The FHD-H is a monomeric cytoplasmic enzyme that contains only one molybdenum centre and one [4Fe-4S] centre. The molybdenum centre is the active centre, where the formate is oxidised, and the Fe/S centre is responsible for the intramolecular transfer to a physiologic acceptor.[22–25] The FDH-N is a complex trimer of trimers ($(\alpha\beta\gamma)_3$) membrane-bound *respiratory* enzyme that harbours two *b* haems, five [4Fe-4S] centres and one molybdenum centre.[16,22] *D. gigas* FDH is a periplasmic dimeric tungsten-containing enzyme that harbours four [4Fe-4S] centres and one tungsten centre. As anticipated, the tungsten centre is the active centre and the Fe/S centre are responsible for the intramolecular electron transfer to a periplasmic c-type cytochrome.[22,26,27]

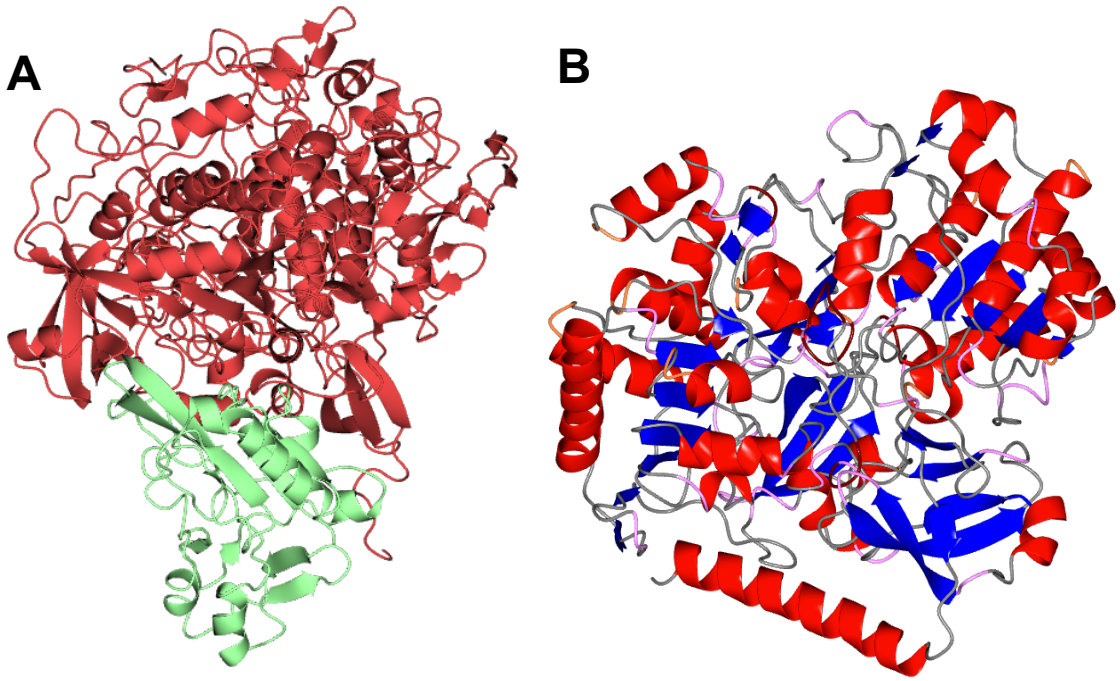

Figure 1.2 Three-dimensional structure views of two FDHs. A - *D. gigas* FDH colored accoring subuntis, with the α subunit in red and the β in green; The structure is based on the PDB file 1H0H. B – *E. coli* FDH H colored accoring structural motifs; α helixes are shown in red and β-sheets are shown in blue;The struture is based on the PDB file 1FDO. The images were produced with CCP4mg molecular-graphics software.

Even though the FDH's structural organization is diverse, the active centre of all currently known metal-dependent FDHs is well conserved.[11,12] The FDHs active site share high primary sequence identity.[28] In the oxidised form, the active site contains one metal ion, molybdenum (VI) or tungsten (VI), coordinated by a cis-dithiolene group of two pyranopterin cofactor molecules (figure 1.3). The metal is further coordinated by one terminal sulfo group and one sulfur or selenium atom from a cysteine or a selenocysteine residue, in a distorted trigonal prismatic geometry (the presence of a cysteine or a selenocysteine residue is dependent on the organism and the reason for this diversity is not yet known).[13,28] The active site also harbours two conserved arginine and histidine residues close to the metal ion, although not involved in the metal coordination, that were suggested to have key roles in catalysis.[23,29]

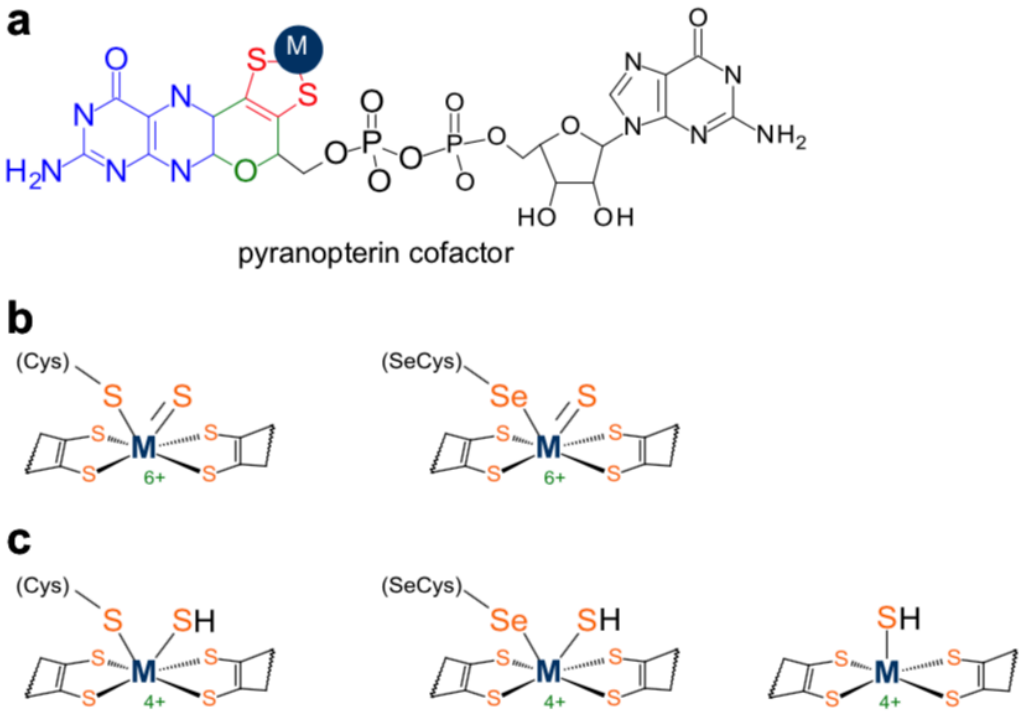

Figure 1.3 The active site of FDH. (a) The structure of the pyranopterin cofactor. The pyranopterin cofactor molecule is formed by pyrano (in green)-pterin(In blue)-dithiolene(in red)-methyphosphate(in black) moieties. The dithiolene forms a five-membered ring with the metal atom (M). (b) Structures of the catalytic centres in their oxidise form (c) Structures of the catalytic centres in a reduce form.[11]

1.2.2 FDH from Desulfovibrio desulfuricans

Desulfovibrio desulfuricans (D. desulfuricans) is a remarkable *Desulfovibrio sp.*, using both sulfate and nitrate as terminal electron acceptors in "respiration". The oxidation of formate by FDHs can be use in electron transfer reactions in both of these pathways.[30] The genome for the *D. desulfuricans* ATCC 27774 codes for three FDHs, with one periplasmic, one membrane-bound periplasm-faced and one cytoplasmic.[31]

Currently, no 3D structure is known for any of the three FDH of *D. desulfuricans*. The periplasmic *D. desulfuricans* FDH contains three different subunits, comprising a molecular mass of 150 kDa; this enzyme contains one molybdenum centre, where formate is oxidised, two [4Fe-4S] centres and four c haems.[32,33] The α subunit (90 kDa) contains the molybdenum centre that holds one molybdenum atom coordinated by four sulfur atoms of two pyranopterin guanosine

dinucleotide cofactor molecules. Completing the metal coordination, there is a conserved selenocysteine residue and a terminal sulfo group (Mo=S), as is suggested by analogy with other FDHs whose structure was determined. The active site pocket is thought to comprise also a conserved arginine and a histidine residues, which were suggested to play a role in catalysis.[23,27] Apart from the molybdenum centre, this subunit also contain one of the Fe/S centres. The β subunit (30 kDa) has the other Fe/S centre and the γ subunit (15 kDa) contains the four c haems.[32]

It has been demonstrated that this enzyme is able to catalyse both the formate oxidation to CO_2 and the reverse reaction of CO_2 reduction, displaying in both cases Michaelis-Menten type kinetics (or saturation kinetics).[34]

1.2.3.Reaction mechanism

The FDH formate oxidation and CO_2 reduction occurs at the catalytic centre (active site) of the enzyme, whether this contain a molybdenum or tungsten ion. Contrary to what is characteristic of most molybdenum- and tungsten-containg enzymes, this reaction does not involve an oxygen atom transfer, because the product of the reaction is CO_2 and not hydrogen carbonate. This was demonstrated when ^{13}C-labelled formate and ^{18}O-enriched water were used, resulting in the formation of $^{13}C^{16}O_2$ gas. [35] Hence, to form CO_2, FDH has to abstract one proton plus two electrons or one hydride from the formate molecule.

Over the years, different mechanistic hypothesis have been proposed in order to explain the catalysis performed by FDHs. These have been based in the structural data of *E. coli* FDH H.[28,29] In 2016, Maia, *et al*[2,34] have proposed a new revised mechanism based on new kinetic and spectroscopic data. According to these authors, the formate oxidation is initiated by formate binding to the oxidised active site, but not directly to the metal atom. It was suggest that it binds to a binding pocket, where a conserved arginine residue (and possibly histidine) anchors its oxygen atom(s) through hydrogen bond(s) and orients its alfa-proton atom towards the sulfo ligand of the molybdenum (or tungsten) centre.[20,21,36] From there, the formate oxidation occurs by hydride transfer from the formate molecule to the sulfo group of the oxidised metal centre, Mo^{6+}=S (or W^{6+}=S), leading to the formation of CO_2 and a protonated sulfo group, Mo^{4+}-SH (or W^{4+}-SH). The catalytic cycle is closed with the oxidation of the metal atom to its initial oxidation state, via intramolecular electron transfer to other redox centres of the enzyme and the molecule of CO_2 being released, as seen in fig.4 (red arrows).[34] Accordingly to this mechanistic proposal, the seleno-cysteine (or cysteine) residue in the active site would remain bound to the metal atom throughout the entire catalytic cycle, that is, the metal atom would remain permanently hexa-coordinated. Yet, the selenocysteine (cysteine) dissociation from the metal is not mandatory for the reaction to proceed by direct hydride transfer, and the catalytic cycle, as suggested, can proceed as well in a penta-coordinated metal centre (fig. 4)[31]. Nevertheless, it can be argued that

a permanent hexa-coordination is essential to prevent the oxygen atom transfer activity that is characteristic of the molybdoenzymes (and tungstoenzymes)[34]. This issue will remain in open until further experimental work sheds light on the fate of the selenocysteine (cysteine) residue during the catalytic cycle.

For the CO_2 reduction, the reverse mechanism was suggested[31] (figure 1.4, green arrows). In this case, the CO_2 would bind to the reduced active site, holding a protonated sulfo group, but not directly to the molybdenum atom. This would happen in the same binding site as for formate, with the same arginine anchoring the oxygen atoms of CO_2, through hydrogen bonds, and forcing its alfa-carbon to point towards the protonated sulfo group. From this point, the carbon dioxide reduction would proceed through a hydride transfer from the protonated sulfo group of the reduced metal centre to the carbon atom of the CO_2 (figure 1.4). The catalytic cycle would be concluded with the reduction of the metal centre, via intramolecular electron transfer from other redox centres of the enzyme and the formate release. [34] What determines the direction of the reaction, formate oxidation *versus* carbon CO_2, is the ability to produce and maintain the metal atom of the active site centre oxidised *versus* reduced and the availability of the substrate, formate *versus* CO_2.[34]

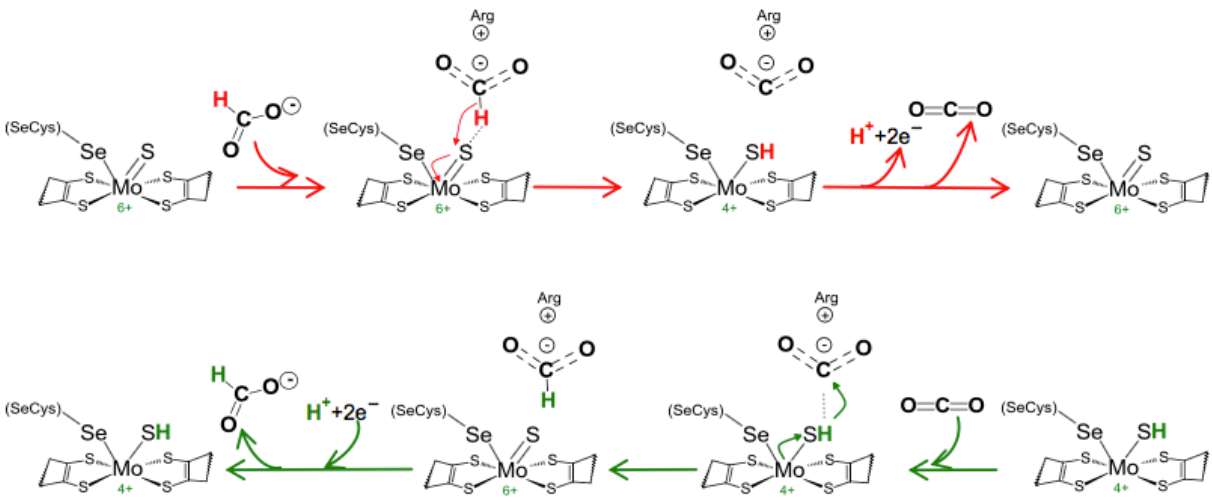

Figure 1.4 Proposed mechanism of formate oxidation (in the red arrows) and carbon dioxide reduction (in the green arrows) catalysed by FDH.[31]

1.3 Electrochemical Studies

1.3.1 Bioelectrochemical methods

When using electrochemistry to study redox enzymes, there are two approaches available: mediated or direct electron transfer methods. Mediated electron transfer uses intermediary redox species to shuttle electrons between the protein or enzyme and the electrode, while in direct electron transfer, the electron transfer occurs directly between the electrode and the enzyme. Considering that proteins and enzymes can have complex secondary and tertiary structures that feature their redox centres internally in their structures, the mediators, usually small redox molecules, are used to facilitate the electron transfer with electrodes since usually may access the buried centres. Mediated electrochemistry has been more used historically when studying the catalysis of these enzymes, since it is easier to obtain results. But when using a mediator to observe a redox reaction, only the influence of the enzyme on the mediator is seen.

Whereas, using the direct approach allows the direct observation of the electrochemistry of the enzyme itself, as well as its catalytic reactions.[37,38] Also, with a direct approach, the redox potential and electron transfer rates can be precisely calculated, which can also help to understand the effects of (bio)environment on the biochemical function of redox enzymes.

1.3.2 Immobilization of enzymes on electrodes

When performing electrochemical studies, the enzyme can either be in solution, as part of the electrolyte, or immobilized on the electrode. Even though having the enzyme in solution is the classical approach, immobilization has some advantages, such as requiring a lesser quantity of enzyme, and in some cases the possibility of its reutilization. Other benefits of immobilization are the reduction of enzyme diffusion, low cost and simplification of the data processing, since the mathematical approach do not take in consideration diffusion of the electroactive species or this is limited (see Appendix).

Direct electrochemical methods have only been successful on a limited number of redox enzymes.

In order to overcome these challenges, there are several immobilization strategies to enhance the communication between the enzyme and electrodes, in order to facilitate the electron transfer process. There are two main strategies in which an enzyme could be immobilized. [37,38]

The first one is physical immobilization methods, in which there are no chemical modifications to the enzyme. This can be achieved with:

- Physical adsorption: this is one of the easiest techniques considering it only requires the enzyme to be deposited within the electrode allowing its adsorption on the surface. However, physical adsorption is a weak interaction and enzymes can in some cases be easily washed out from the surface or denature through this process. [38,39]
- Physical immobilization or entrapment: here the enzyme solution is added to the surface of the electrode and trapped there by a porous membrane (with a suitable cut-off). This forms a thin layer of solution (with thickness typically under 100 micrometres), that are allowed to be instantly electrolysed, and where the diffusion of the electroactive species can be considered negligible. This technique keeps the enzyme from diffusing away from the electron surface (washing out). However, if the membrane is too thick, it might be difficult to the substrate to diffuse across the porous membrane, and as so, this have to be carefully chosen. Another point to take into consideration when using a membrane is that, the surface of the membrane also has a charge and therefore electrostatic bonds/repulsions may occur. [38,39]
- Encapsulation: encapsulating the enzyme in a matrix, such as a conducting polymer, sol-gel materials or by binding to nanoparticles, such as gold and platinum, provides a structural entrapment without covalent binding. This technique can provide stabilization to the enzyme, but the matrix can hamper the transport of the substrate and the product, for instance, in and out the polymer.[38,40–42]

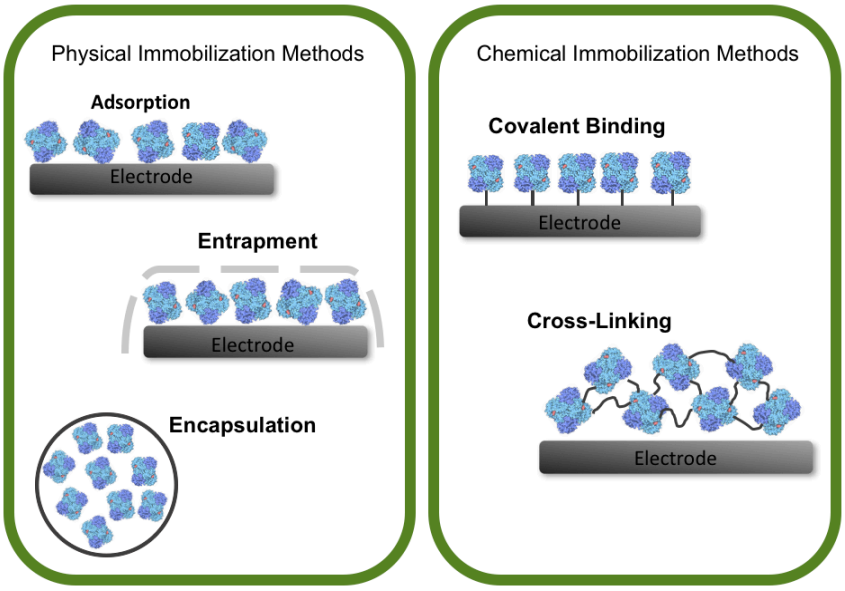

Figure 1.5 Schematization of the diferent types of proteins' immobilization

The second immobilization method is chemical. This can be accomplished by either covalent binding the enzyme to surface of the electrode (modified) or to polymers that act as immobilization matrices (cross-linking). This technique has little loss of enzyme but as a result of the covalent binding, often the specific activity of the enzyme decreases due to formation of additional chemical links.[38,39]

1.3.3 Review of FDH electrochemical studies

Even though there was some research into FDH in the past, that mainly focused on its structure and the mechanism of its catalysis of formate oxidation, in the last few years, there has been an increase of attention specially dedicated towards the reversibility of the FDH's catalysis and the possibility of new environmental applications.[43–46] Most have been conducted using EPR and crystallography, although a few have used mediated electrochemistry as a method of study. These enzymes are suitable for adsorption onto an electrode that is able to mimic its physiological partners. This way, the electrode is able to accept the electrons from the formate oxidation, and it also may donate electrons for the CO_2 reduction.[47–50]

Considering it was thought that FDH that contained tungsten in its active site could be more efficient at reducing CO_2, there was a larger focus on these[51]. Hirst *et al*[50] have been using W-dependent FDH *from Syntrophobacter fumaroxidans* with some success, adsorbing it on the graphite electrode surfaces and observing its catalytic activity towards CO_2 reduction by using mediators. Also, Kano *et al*[48] have been studying the CO_2 reduction using a W-FDH from *Methylobacterium extorquens* by modifying electrodes' surfaces and using different mediators, like methyl viologen. But all of these studies use mediated electrochemistry, until this point, there has not been reported a successful FDH study by direct electrochemistry.

2. Objectives

For many years, our research group has studied the enzymes from *D. desulfuricans*. With the current pressures in finding alternative ways to combat climate change, there has been a renewing interest in FDH due to its capabilities of reducing CO_2 to formate. It is in this framework that this Thesis finds its main target: purify the *D. desulfuricans* FDH and characterise electrochemically the enzyme redox centres using a non-mediated direct electrochemical approach, in order to determine redox features like formal potential, as well as evaluate the *D. desulfuricans* FDH catalytic behaviour towards the CO_2 reduction.

3. Materials and Methods

3.1 Purification of FDH

3.1.1 Protein Purification

The *D. desulfuricans* FDH purification process was performed as previously described[32] and all purification procedures were performed under aerobic conditions at 4ºC. In figure 3.1, a flowchart summarises all the purification steps.

The *D. desulfuricans* ATCC27774 bacterium was grown in a vitamin/nitrate culture media, in a 300L reactor, under anaerobic conditions, at 37ºC, and the cells were collected by centrifugation. The cellular growth resulted in 640g (wet weight) of cells. The cells were suspended in 10 mM Tris-HCl pH 7.6, in a ratio of 1:2 (cells:buffer), and disrupted in a French Press at 9000 psi. The cellular extract was centrifuged (10 000g for 45 min), to eliminate the cellular debris, and ultracentrifuged (180 000g for 60 min), to separate the membrane fraction. The resulting supernatant was dialyzed overnight against 10 mM Tris-HCl pH 7.6 buffer, with 5 kDa cut-off membranes. The cellular extract thus obtained was subjected to three chromatographic separation procedures.

The cellular extract was first separated in an anionic exchange column of DE-52 (Whatman BioProcess resins, ∅=5cm and h=29cm), previously equilibrated with 10 mM Tris-HCl pH 7.6. The FDH was eluted using a NaCl gradient of 0-500 mM (in 3.5 volumes). The fractions displaying FDH activity were pooled and concentrated using a ultrafiltration concentrator, with a 5kDa cut-off membrane, and subsequently dialyzed overnight against 10 mM Tris-HCl pH 7.6 buffer. The next step on the purification procedure was a second anionic exchange chromatography in a column of Q-Source (GE, ∅=2.6cm and h=23.5cm) equilibrated with 10 mM Tris-HCl pH 7.6 buffer. FDH was eluted using a linear gradient of NaCl of 0-500 mM (in 5 volumes). The fractions exhibiting higher FDH activity were collected and concentrated using an ultrafiltration concentrator, with a 5kDa cut-off membrane, and subsequently dialyzed overnight against 100 mM Tris-HCl pH 7.6 buffer. The third chromatographic step was a hydroxyapatite column (Bio Rad Bio-Gel HTP, with ∅=2.6 cm and 24.5cm), equilibrated with 100 mM Tris-HCl pH 7.6 buffer. FDH was eluted with a linear gradient of potassium phosphate of 0-200 mM (in 5 volumes).

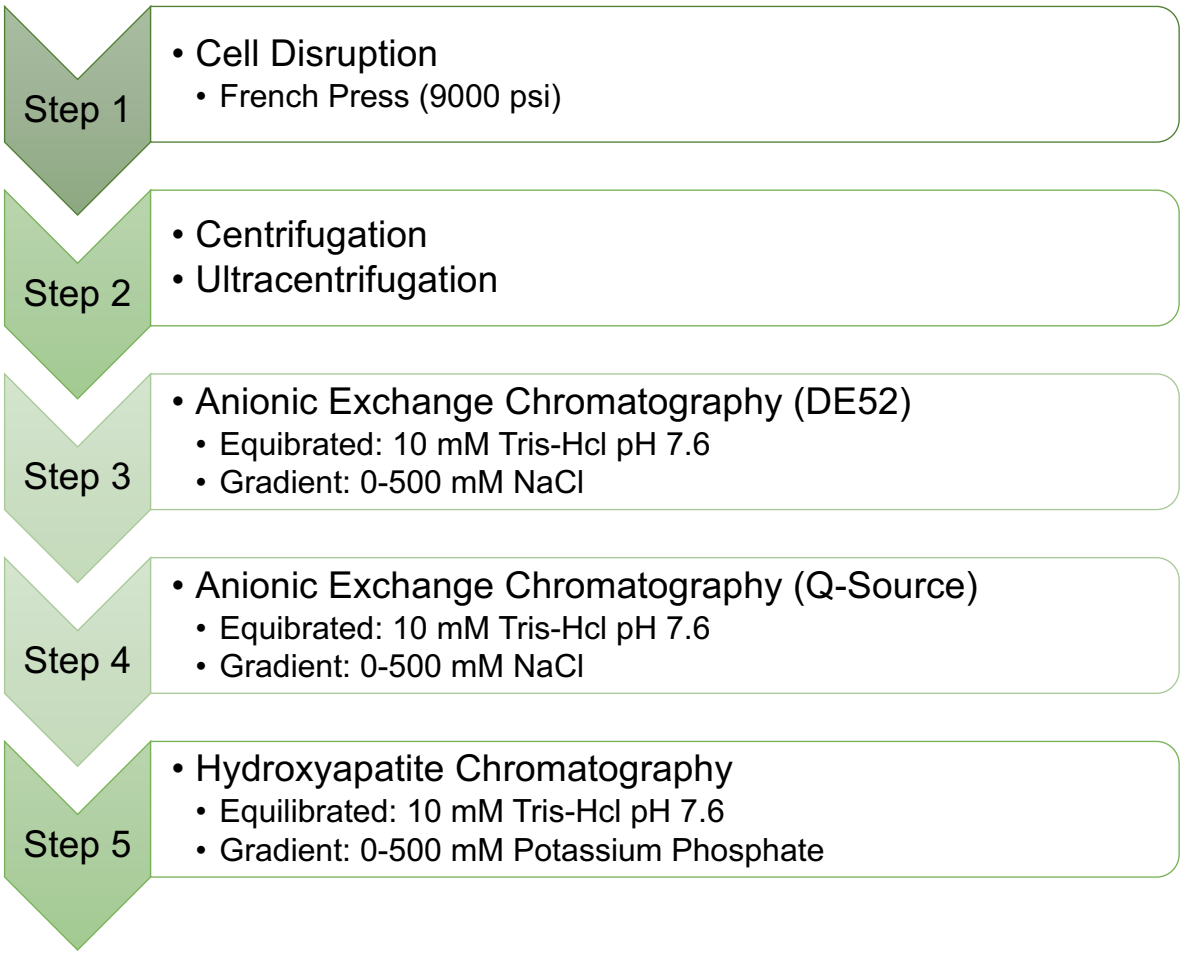

Figure 3.1 Flow chart summarising all the purification steps of FDH from *D. desulfuricans* ATCC 277747

3.1.2 Protein Quantification

In order to quantify the total concentration of protein in the samples, a modified version of the Lowry/Biuret method was employed, using bovine serum albumin as a standard protein (details in Appendix.)

3.1.3 Activity Assays

To follow the FDH purification process, two types of enzymatic assays were performed, both based on the oxidation of formate to carbon dioxide: an *in-gel* activity assay and a "classic" spectrophotometric activity assay.

The "classic" spectrophotometric assay is a quantitative assay, where the anaerobic oxidation of formate is evaluated following spectrophotometrically the reduction of benzyl viologen (BV; equation 2) at 555 nm (ε=12 $mM^{-1}cm^{-1}$). For that, the enzyme sample was incubated with 10 mM formate and 2 mM dithiothreitol, in 60 mM Tris-HCl pH 8 buffer, during 30 minutes, at room temperature, under a argon atmosphere (to remove the dioxygen from the reaction mixture and create the necessary anaerobic conditions). The reaction of formate oxidation was initiated by the addition of 7.5 mM BV. One unit of enzyme activity was defined as the amount of sample that catalyses the oxidation of 1μmol of formate per minute.

$$HCOO^- + 2BV(oxi) \rightleftharpoons CO_2 + 2BV(red) \qquad \text{Eq. 2}$$

The *in-gel* activity assay is a qualitative assay, where the anaerobic oxidation of formate is evaluated following visually the reduction of methyl viologen (MV; equation 3) in a polyacrylamide gel that was previously subjected to an electrophoresis under native conditions (Native-PAGE). For that, the FDH samples were first separated by Native-PAGE (as described below, under section 2.2.4). All gel lanes contained the same protein concentration (determined as described above, in 2.2.2). The polyacrylamide gel was subsequently incubated with 10 mM formate and 130 mM of β-mercaptoetanol, in 60 mM Tris-HCl pH 8, during 20 minutes, under argon atmosphere (to create the necessary anaerobic conditions). The reaction of formate oxidation was initiated by the addition of 7.5mM MV. In the gel lanes containing FDH, MV would be reduced (equation 3) and a blue band would be developed (while the oxidised MV has no color, the reduced MV is blue).The size of the blue band would indicate, qualitatively, the amount of FDH present in that sample. Subsequently, to "fixate" the blue bands (to avoid the diffusion of the reduced MV and, thus, preserve the "gel activity coloration"), 2,3,5-triphenyltetrazolium chloride was added and incubated for more 10 minutes. This tetrazolium precipitates in the gel when it is reduced at the expenses of MV re-oxidation, transforming the blue bands into red ones (the tetrazolium develops a red colouring when reduced).

$$HCOO^- + 2MV(oxi) \rightleftharpoons CO_2 + 2MV(red) \qquad \text{Eq.3}$$

3.1.4 Electrophoretic analysis

The FDH purification process was also followed by polyacrylamide gel electrophoresis, in the presence of sodium dodecyl sulfate, under denaturating conditions (SDS-PAGE). The SDS-PAGE was preformed according to the Laemmi protocol[52], using a 5% stacking gel and a 12.5% separating gel. All the samples were diluted (1:1) in sample buffer containing 1% of sodium dodecyl sulphate (SDS), 5% of β-mercaptoetanol, 80 mM Tris-HCl pH 6.8, 0.01% bromophenol blue and 10% of glycerol and heated during 5 minutes at 100ºC. The molecular mass standards use were Xylanase U4 (96 kDa), Albumin (66 kDa), Phosphomanose Isomerase (48 kDa), Cellulase 5A (40 kDa), Cellulase M9 (32 kDa), Family 4 Carbohydrata esterase (26 kDa) and Xyloglucan-Binding Domain M6 (18.5 kDa).

For the *in-gel* activity assays, Native-PAGE was used. For this type of electrophoresis, a 5% stacking gel and 12.5% separating gel were used. All the samples were diluted (1:1) in sample buffer containing 80 mM Tris-HCl pH 6.8, 0.01% bromophenol blue and 10% of glycerol. During the Native-PAGE, markers were not used.

3.2 Electrochemical measurements

The electrochemical assays were performed using an Autolab PGSTAT12 (Autolab) potentiostat/galvanostat and GPES (version 4.9) as the data acquiring software. The FDH characterisation assays were conducted in a single compartment cell with a three-electrode configuration, inside a Faraday box and at room temperature (23ºC). The three-electrode cell was consisted in a pyrolytic graphite disk (3 mm diameter) working electrode, a saturated calomel electrode (SCE) and a platinum wire electrode, used as reference and secondary electrodes, respectively. Before each experiment, all solutions were degassed for 30 min and after the cell was kept in a positive atmosphere of argon.

For each experiment, the working electrode was polished with both 1 μm and 0.3 μm alumina for 10-15 minutes each. After rinsing with MilliQ water, the electrode is placed in an ultrasonic bath for 3-4 minutes. Then, it is thoroughly rinsed again with MilliQ water and left to dry at room temperature.

A 5 μl of FDH (7.9 μM) was placed on the surface of the electrode and, using the solvent casting technique, was left to slowly dry during approx. 5 minutes, till it reaches half the initial volume. Then a cellulose membrane (Spectra Por3 with a 3.5 kDa cut-off) was applied on the

surface of the electrode in order to immobilize the enzyme. The membrane was kept in place with an O-ring and a rubber bland and sealed with Teflon tape.

The first experiments were performed using a 20 ml buffer solution of 300 mM of Tris-HCl, pH 7.6, and 100 mM of KNO_3, as supporting electrolyte. But taking in consideration that in the literature some reports indicated that nitrate might be an inhibitor for other FDH[53], the same assays were performed changing this salt to 100mM of NaCl. In the pH dependence studies, in order to expand the values of pH, the buffer was change from Tris-HCl to a mixture of 300 mM of TRIS-Citric Acid. For the catalysis' assays, solutions of 10 mM sodium formate and 10 mM sodium carbonate were prepared in MilliQ Water.

The redox potential values were converted from SCE to NHE, taking in consideration the temperature dependence, using Eq.4 and are presented in this later reference scale.

$$E\ (V) = 0.2412 - 6.61\times10^{-4}(T - 25ºC) - 1.75\times10^{-6}(T-25\ ºC) – 9\times10^{-10}(T - 25\ ºC) \quad \text{(Eq.4)}$$

4. Results and Discussion

4.1 Purification of FDH

The FDH was purified from *D. desulfuricans* cells using several centrifuge and chromatographic separation procedures (Fig. 3.1). The centrifuge steps eliminated the cellular debris and the membrane fraction. The first chromatographic process, an anionic exchange chromatography performed in a column with a large volume of DE-52 (Whatman BioProcess resins), operated under gravity (without using a pressure pump), aimed to do a first, "coarse cleaning" of the cellular extract, which had a large volume. As expected from previous purifications processes, FDH was eluted during the gradient stage of the chromatography, at around 150 mM NaCl (NaCl concentration at the entrance of the column).

The next step was another anionic exchange chromatography, in this case in a Q-Source (GE) column. FDH was eluted in the gradient phase, at around 180 mM of NaCl, (figure 4.1). This chromatographic separation resulted in a purification of 15 times, with a very significant FDH recovery (55%) (Table 4-1).

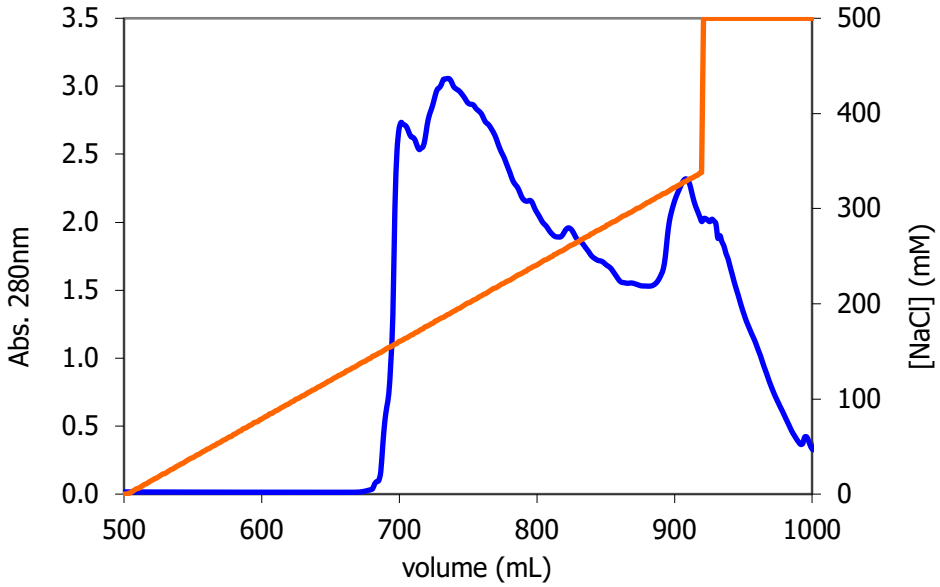

Figure 4.1 Chromatogram of the separation of the FDH extract in a Q-source column, during the NaCl gradient phase. The blue line represents evolution of the Abs at 280 nm and the orange line represents the progression of the NaCl gradient. Details of the separation procedure can be found in section 3.1.1.

The next step in the FDH purification was a hydroxyapatite chromatography. As expected, the enzyme was eluted in the gradient phase, at around 100 mM of potassium phosphate (figure 4.2). It is to be noted that no large loss of enzymatic activity occurred during this step, as some authors had reported, with the step resulting in a 17% yield (Table 4-1). In addition, this chromatographic step greatly increased the purity of the sample (120 times). Further confirmation of the high purity of this FDH sample came from the electrophoretic analysis under denaturating conditions, SDS-PAGE (figure 4.3), where it is possible to clearly observe the three bands, corresponding to the three *D. desulfuricans* FDH subunits, free of major contaminants.

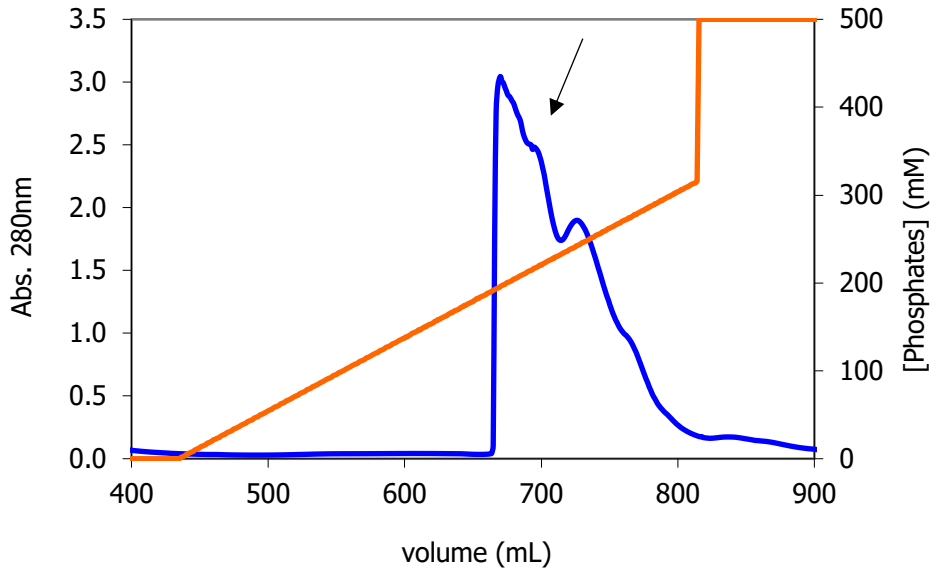

Figure 4.2 Chromatogram of the separation of the FDH extract in a hydroxyapatite column, during the phosphate gradient phase. The blue line represents evolution of the Abs at 280 nm and the orange line represents the progression of the phosphate gradient. The black arror indicates the peak corresponding to FDH. Details of the separation procedure can be found in section 3.1.1.

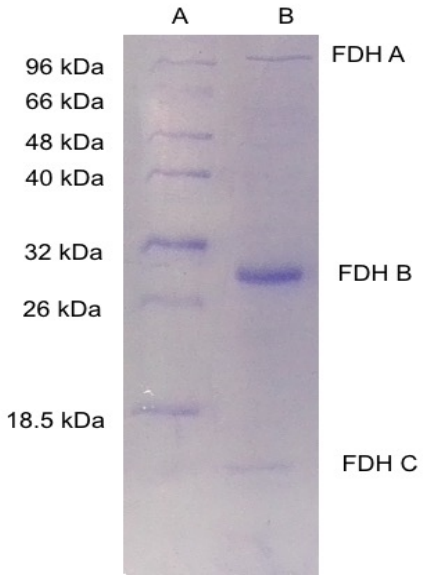

Figure 4.3 Electrophoretogram of the separation under denaturating conditions (SDS-PAGE) of the most purified FDH fraction after the HTP chromatography – A is the molecular mass markers (whose masses are indicated) and B the most purified FDH fractions (where the bands corresponding to the three subunits of FDH indicated). Details of the electrophoresis procedure can be found in 2.2.4.

Table 4-1 summarises the results obtained during the *D. desulfuricans* FDH purification process. Due to an error, resulting in the loss of a viable sample, it was not possible to determine the activity of the FDH sample eluted from the DE-52 column. Overall, the purification procedure implemented allowed the purification of FDH about 120 times, with a yield of 140 mg (17% recovery) and a specific activity of 21.9 U/mg. Even thought, this purification resulted in a FDH sample with a lower specific activity comparatively to what was described previously.[33]

Table 4-1 Purification of formate dehydrogenase from *D. desulfuricans* ATCC 27774

Purification Step	Total Protein (mg)	Total Activity (U)	Specific Activity (U/mg)	Purity (x)	Yield (%)
Soluble Extract	101×10^3	18.4×10^3	0.182	1	100
DE-52	12.1×10^3	-	-	-	-
Q-Source	3.73×10^3	10.1×10^3	2.71	14.9	54.9
HTP	140	3.06×10^3	21.9	120	16.6

4.2 FDH Electrochemical Characterisation

The first aim to be attempted was the FDH characterisation by cyclic voltammetry in non-turnover conditions, aiming to obtain a direct electrochemical response of the enzyme. The representative voltammogram in figure 4.4 depicts this.

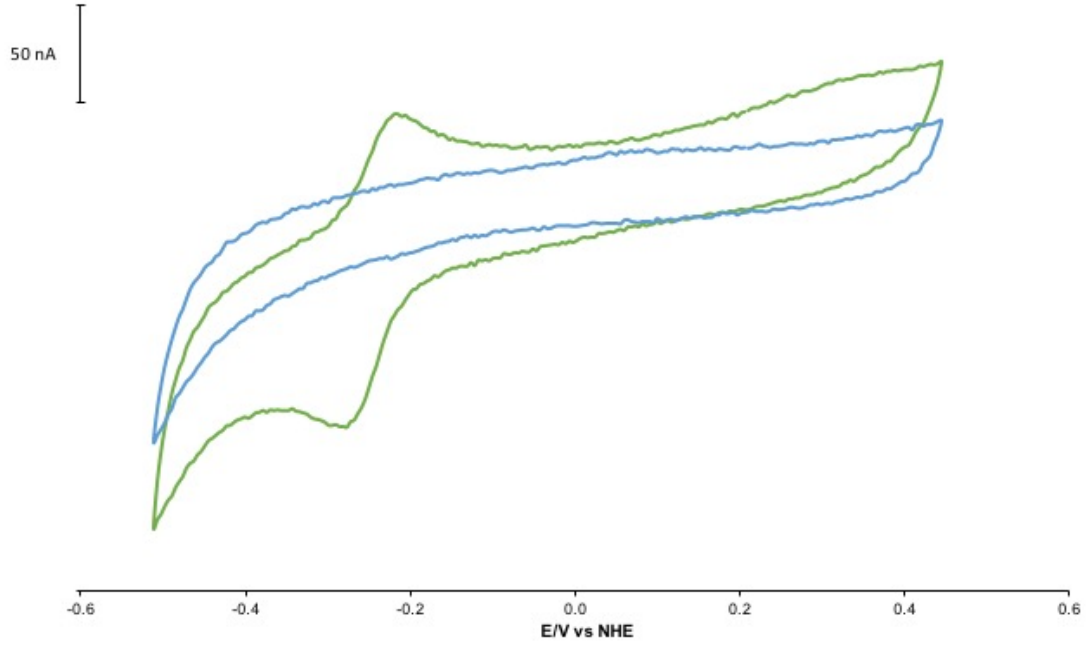

Figure 4.4 Typical cyclic voltammogram of 7.9 uM FDH (Green line) and the blank (Blue line). The assay was done in 300 mM Tris-HCl pH 7.46; 100 mM KNO_3 at v = 10 mV/s.

In the FDH voltammogram, obtained at 10 mV/s, a redox pair is observed that, by comparing with the control, was assigned to FDH. The anodic and cathodic current peaks were observed approx. at the average values of -212 mV and -279 mV, respectively, corresponding to a formal potential of -0.245 ± 0.008 mV vs NHE, calculated by the average of the two potentials, ($\frac{E_{pa}+E_{pc}}{2}$). Considering that this pair of signals is within the range of molybdenum signal reported in the literature[53] and later, in the catalytic assays the current variations are seen at potential values corresponding to this redox pair during the reduction of CO_2 (described and analysed in section 3.3), we have assigned these signals to molybdenum redox pair of the active centre, Mo(IV/VI). The other anodic peak, visible around +332 mV vs NHE is less defined than the other two, and the corresponding cathodic counterpart is not observable at these experimental

conditions. The voltammetric results and its comparison with the controls, show that direct electron transfer between the redox centres of FDH and the surface of the electrode was successfully accomplished.

As was previously mentioned, the electrolyte was changed from containing KNO_3 to NaCl due to the possibility of the nitrate being an inhibitor. In such a way, the tests were repeated, leading to the possibility of comparison, as can be seen in the figure below.

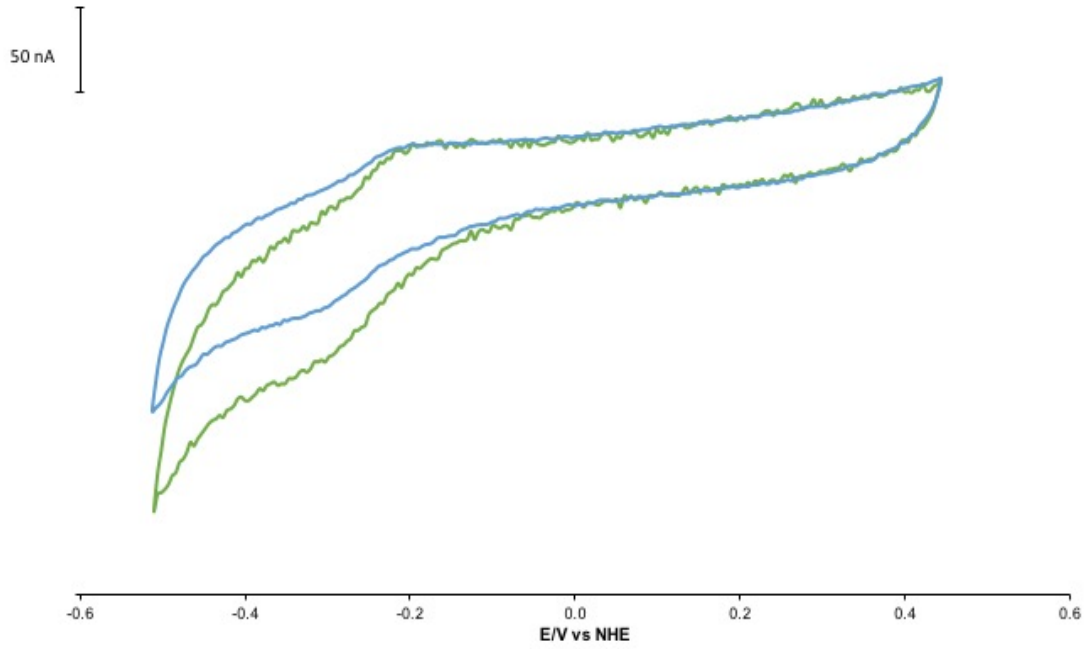

Figure 4.5 Cyclic voltammetry of FDH; Assay conducted using KNO_3 (Blue line) or NaCl (Green line), as supporting electrolyte; v = 10 mVs^{-1} for both assays.

Comparing the two voltammograms, it is possible to distinct areas of comparison, one where the two voltammograms are completely matched (at more anodic potential values) and a second, where the voltammogram conducted using NaCl as supporting electrolyte is shifted down, presenting a higher cathodic current, comparing to the one performed with KNO_3. This difference could be the result of different factors that can affect the preparation of the assay, like the different presence of residual air in the assays. Even though, they aren't completely matched, it is possible to see that both currents peaks seen, in both graphs, occur at similar potential values. In order to be able to compare the intensity of the redox pair in both voltammograms, the ratio I_{pa}/I_{pc} was calculated. While both were considered similar, since the value for the assay with NaCl was 0.98 ± 0.05 and with KNO_3 was 1.1 ± 0.06, the peaks for the assays conducted with NaCl are slightly more intense.

Bearing in mind that both of these assays were conducted without the presence of substrate, a part of the CO_2 naturally dissolved in solution, it is possible to conclude that the presence of nitrate on the electrolyte does not interfere with the electrochemical characterisation of this FDH.

In order to optimize the process of characterisation, several assays were conducted in order to find the most adequate window that shows all the redox processes. The chosen window was between -510 and 400 mV vs NHE in order to be able to observe both process that had been identified. With that step concluded, a number of assays were made at different scan rates, as seen in figure 4.6. Different scan rates can show different redox processes due to the different electrochemical behaviour that those may present (higher or lower electron transfer constants). For the FDH system, and in particular for the redox pair assigned to the Mo centre (the more negative process), the optimal scan rate was found to be 10 mVs^{-1}, at the applied experimental conditions. With lower scan rates, the plots were compromised with electric noise and at higher rates, the signals were less defined.

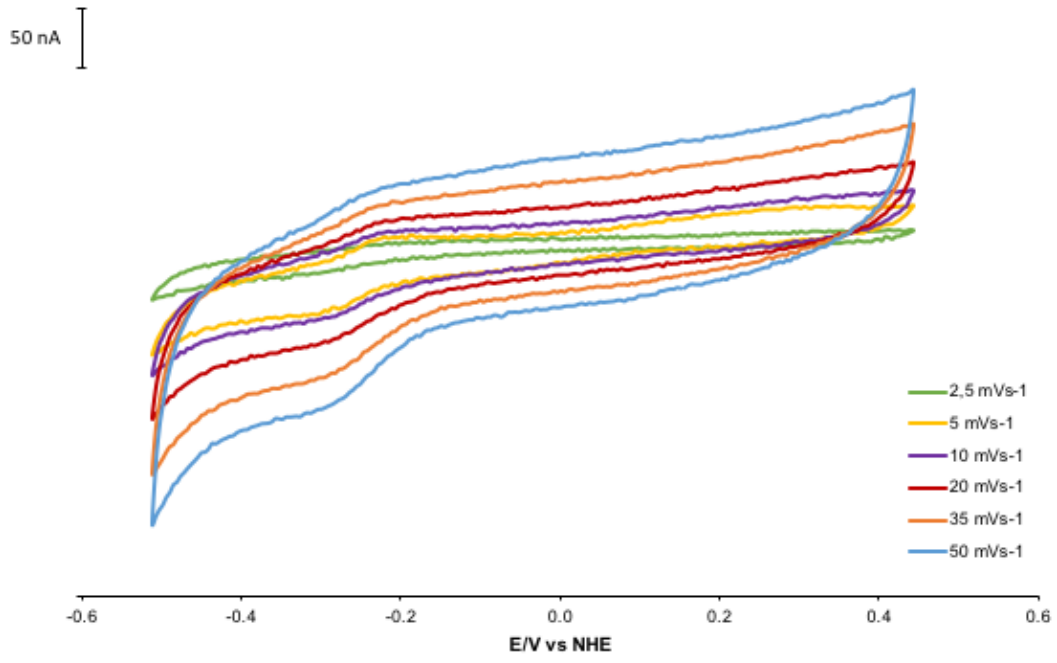

Figure 4.6 Cyclic voltammograms of FDH at different scan rates; all assays were conducted in 300 mM Tris-Citrate pH 7.5; 100 mM NaCl

With these assays shown in figure 4.6, several parameters needed in the FDH characterisation were obtained and calculated. These consisted in both cathodic (E_{pc}) and anodic peak (E_{pa}) potentials and their corresponded cathodic (I_{pc}) and anodic (I_{pa}) peak currents, which are shown in table 4-2 along with their Standard Deviation (SD). In table 4-3, the I_{pa}/I_{pc} ratios,

formal potential ($E^{0'}$), the number of electrons (n) involved in the redox transition and ΔEp, which is calculated by the difference of the cathodic and anodic peak potentials, are shown. These parameters were taken only for the process assigned to the Mo centre (the more negative process in the voltammograms) and give important information on the system reversibility.

Table 4-2 Current peak (Ip) and Potential of the FDHs peaks at diffent scan rates with correspondent Standart Deviation (SD)

v (V/s)	E_{pa} (V)	SD	E_{pc} (V)	SD	I_{pa} (A)	SD	I_{pc} (A)	SD
0.0025	-0.207	0.018	-0.278	0.027	$3.37x10^{-09}$	$8.0x10^{-10}$	$-1.1x10^{-08}$	$4.29x10^{-09}$
0.005	-0.211	0.018	-0.278	0.027	$1.08x10^{-08}$	$3.1x10^{-09}$	$-1.8x10^{-08}$	$4.85x10^{-09}$
0.01	-0.204	0.011	-0.271	0.011	$1.88x10^{-08}$	$1.0x10^{-08}$	$-3.3x10^{-08}$	$1.60x10^{-08}$
0.02	-0.205	0.016	-0.280	0.012	$1.28x10^{-08}$	$6.6x10^{-09}$	$-3.3x10^{-08}$	$8.03x10^{-09}$
0.035	-0.202	0009	-0.278	0.005	$1.39x10^{-08}$	$7.6x10^{-09}$	$-4.5x10^{-08}$	$7.52x10^{-09}$
0.05	-0.222	0.002	-0.280	0.007	$6.46x10^{-09}$	$3.5x10^{-10}$	$-4.0x10^{-08}$	$4.48x10^{-09}$

Table 4-3 Values of Ipa/Ipc, E°', ΔEp and n for each scan rate with Standart Deviation

v (V/s)	Ipa/Ipc	SD	E°' (V)	SD	ΔEp(V)	SD	n
0.0025	0.320	0.060	-0.242	0.022	0.071	0.009	1.276
0.005	0.780	0.040	-0.244	0.022	0.067	0.009	1.362
0.01	0.580	0.040	-0.238	0.011	0.067	0.000	1.352
0.02	0.390	0.110	-0.242	0.014	0.075	0.004	1.208
0.035	0.310	0.120	-0.240	0.007	0.076	0.005	1.200
0,.05	0.160	0.010	-0.251	0.004	0.058	0.005	1.576

This system has a formal potential on average of -245 ± 8 mV vs NHE, as it was mention above, in section 4.2.

As seen in table 4-3, one of the parameters calculated was the number of electrons transferred for the process (n). This was calculated using the equation $\Delta Ep=57/n$.Considering that the process that is being observed is the molybdenum atom going from Mo(IV) to Mo(VI), it should be expected a value of n to be 2. The values approach this value only at the scan rate of 50 mVs^{-1}, leaving to conclude that the 2 electron transfer happens quickly and only can be seen when using faster scan rates, or that the Mo(V) intermediate state is unstable and rapidly becomes Mo(VI).

4.2.1 Study of the reversibility of the FDH system

One of the important steps in the characterisation of FDH was the diagnostic of the electrochemical system. Considering the type of immobilized used, a thin layer electrochemical system, the criteria applied for the diagnostic were the appropriate for this diffusionless technique. The reversibility criterial for cyclic voltammetry in a thin layer electrochemical system can be found in the appendix.

For the first criteria of reversibility to be met, a linear behaviour of the plot of current intensity (I_p) versus the scan rate (v) is needed. In figure 4.7, is possible to see that is not the case for every scan rate. At lower scan rates, typically until 10 mVs^{-1}, there is a linear behaviour. At scan rates above 10 mVs^{-1}s, the linear behaviour is no longer seen. This could be due to an increased irreversibility of the system or may also indicate a low electron transfer constant rate (k_{sh}).

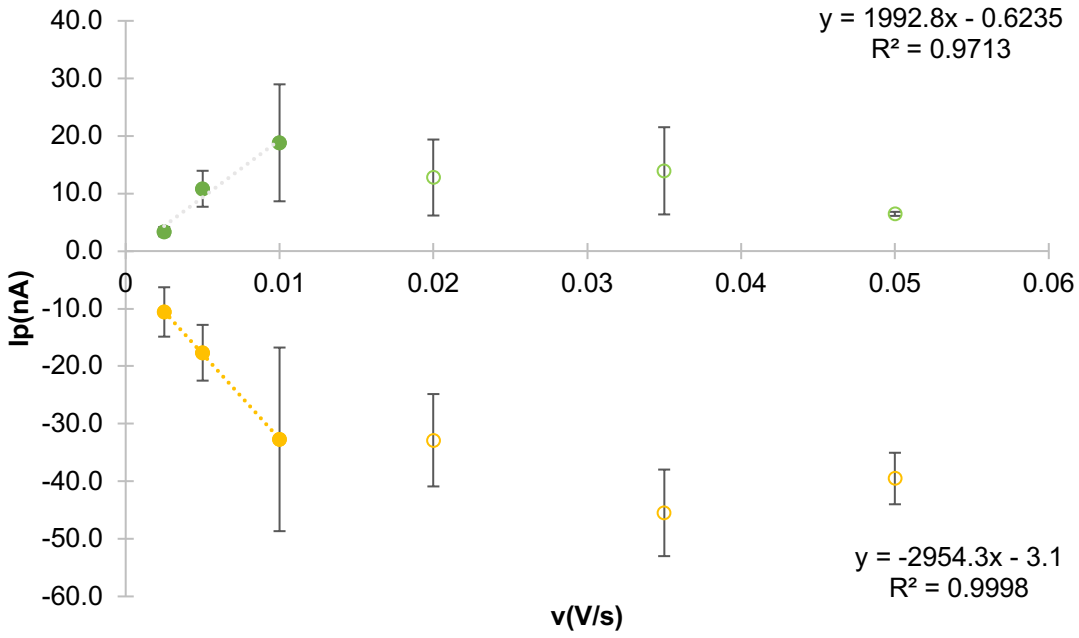

Figure 4.7 Plot of current intensity vs scan rate; The I_{pa} are shown in Yellow and the I_{pc} are shown in Green. Only the full dots are considered for the trendline.

Another criterion of reversibility is the dependence of the difference of the potential values (ΔE) with the scan rate. Again, in a full reversible system, the expected was a linear behaviour. As seen in figure 4.8, this only happens for scan rates until 20 mVs^{-1} if one excludes the point at 2.5 mVs^{-1}, due to the increase of the irreversibility of the system. Once again, this criterion is not fully met.

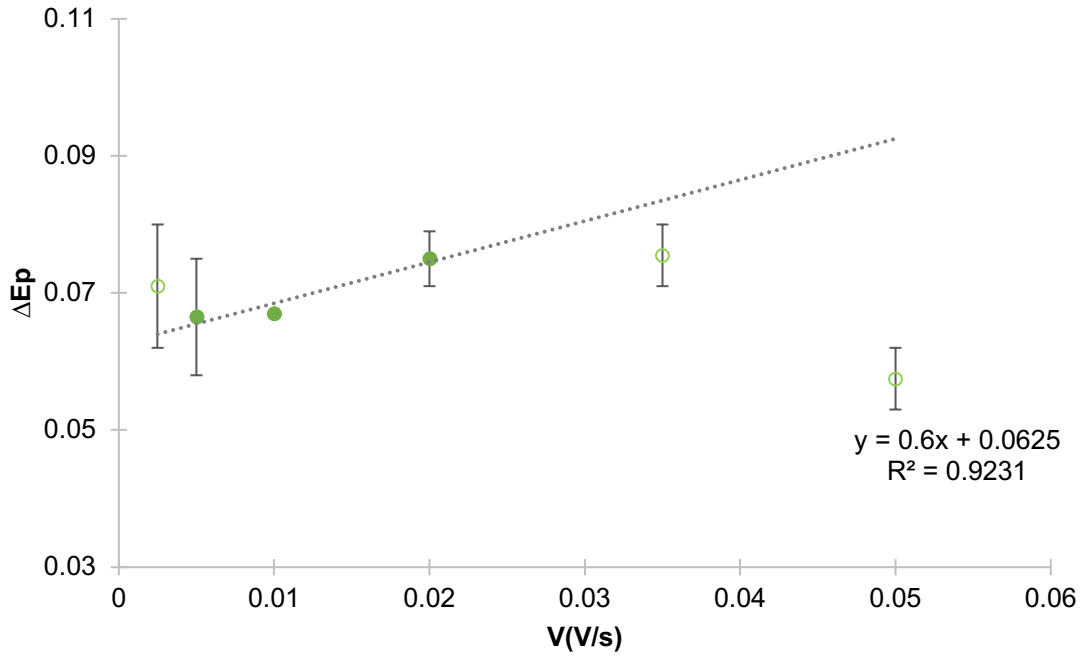

Figure 4.8. Plot of potential diference versus scan rate; Only the full dots are concidered for the trendline. The values of Ip were taken from the scans shown in figure 4.7.

The last criterion, which is partially met, implies the value of I_{pa}/I_{pc} to be approx. 1. The calculated value for this criterion was 0.58 ± 0.04, using a scan rate of 10 mVs^{-1}. During the assays there may have been some residual CO_2, which may have triggered some residual catalysis leading to a higher value of I_{pc}.

Considering that not all of the reversibility criteria were met, it is possible to conclude that the FDH system can be considered as a quasi-reversible system which is common in proteins. Although not being a complete reversible system, during this work it was considered as such by approximation at scan rates from 2.5 to 10 mVs^{-1}.

4.2.2 Electron transfer kinetics of FDH

The rate of electron transfer between an electrode surface and the redox system is another important step in the characterisation of this system. In order to determine the heterogeneous electron transfer rate constant of the system (k_{sh}), Laviron's mathematical approach was used (described in Appendix). In this approach, two methods are described in order to calculate k_{sh}, one for systems with ΔEp higher than 200 mV and a second where this parameter is less than 200 mV. [54]

Considering that the values of ΔEp were lower than 200/n mV, the method 2 of the Laviron's mathematical approach was used to calculate k_{sh}. The different values of k_{sh} at different scan rates, seen in table 4-4, where calculated assuming n=2. These values are relatively low and point to a relatively slow electronic kinetic transfer system, in agreement with the best scan rate found to observe the redox pair (10 mVs^{-1}), where the results obtained with the slower rate voltammograms, have much better defined redox peaks than the ones obtained at higher scan rates. For the best scan rate found, the value of k_{sh} was 0.06 $cm.s^{-1}$.

Table 4-4 Values of k_{sh} comparing with the scan rate

v (Vs^{-1})	ΔEp (mV)	nΔEp	m	k_{sh} (cms^{-1})
0.0025	71	142	0.20	0.02
0.005	66.5	130	0.17	0.03
0.01	67	134	0.16	0.06
0.02	75	150	0.15	0.11
0.035	75.5	151	0.13	0.18
0.05	57.5	115	0.13	0.25

4.2.3. FDH Electroactive Concentration

The number of electroactive molecules on the electrode was estimated through the number of immobilized FDH molecules inside the membrane volume. This was obtained by applying Faraday's laws of Electrolysis. The following equation was used:

$$Q = n\,F\,m \qquad \text{Eq. 5}$$

where Q is the total electric charge passed through the electroactive species, F is the Faraday constant (F=96485.33 A/mol) and m is the number of mol of the total of electroactive molecules (mol).

Q can be obtained by calculating the area of the redox peaks when the voltammogram is displayed in a graph of intensity versus time (Q = I x t). In this case, Q was obtained automatically

though the GPES software by integration of the voltammograms peaks' areas. Also, n was considered as two, following the considered reaction Mo(IV)↔Mo(VI). At a ν = 10 mVs^{-1}, the calculated average number of mol of the total electroactive molecules is 1.94e-13 mol.

Ip = f(v) slope, using the following equation:

$$I_p = \frac{n^2 F^2 \nu V [O]_i}{4RT} \qquad \text{Eq. 6}$$

where Ip is the anodic peak current (A), n is the number of electrons transferred, V is the volume (m^3), [O] is the concentration for the enzyme (oxidized) solution (mol/m^3), ν is the scan rate (V/s), and R, T and F are gas, temperature and Faraday constant, respectively (R = 8.314 $Jmol^{-1}$ K^{-1}, T = 296 K, F = 96485.33 A mol^{-1}).

In order to calculate the volume of the thin layer, the slopes of the linear equations seen the figure 4.7 where used, and n equals 2 and the concentration for the enzyme was 7.926 μM. The calculated volume for the average between the cathodic and anodic peaks was 0.124 μL, a value that, although still in agreement with the thin layer conditions, may be considered low.

4.2.4 Study of the pH dependence of the Mo redox centre

The last system characteristic studied in the FDH characterisation was the pH dependence of its Mo redox centre. For that it was chosen four different pH values to test its influence. Figure 4.9 depicts the evolution of the FDH signal with the different pH values. It is possible to observe a shift in the peaks as the values of the pH changes. This deviation could be due to a protonation or deprotonation on the active centre that influences the signal.

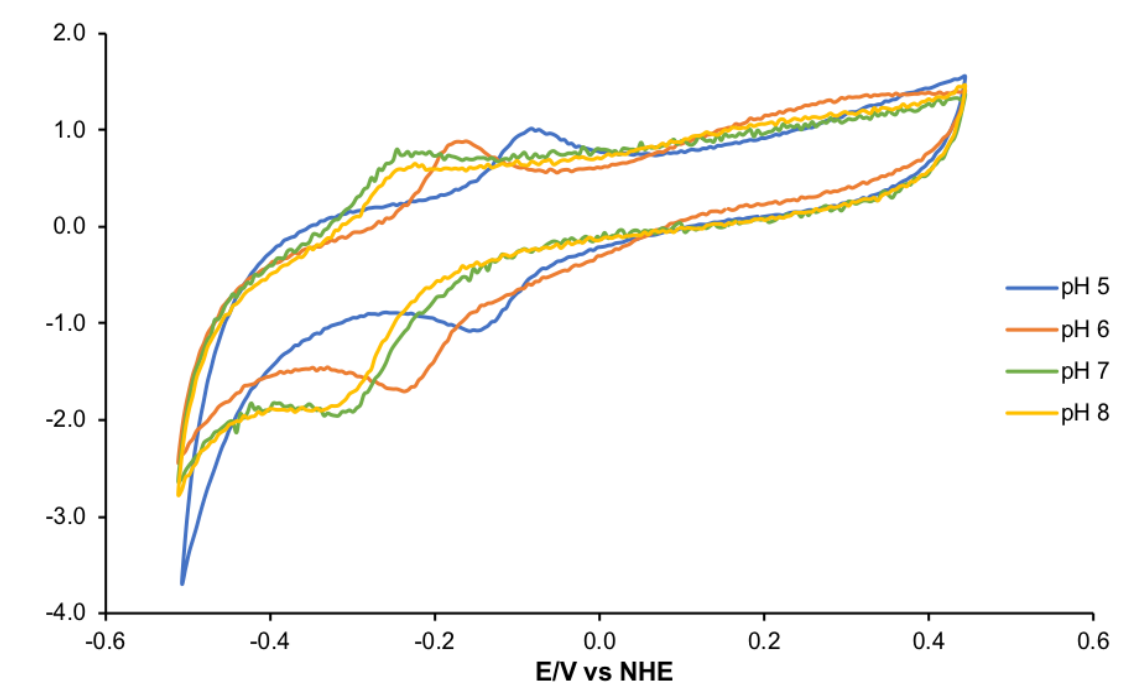

Figure 4.9 Cyclic voltammograms at different pH; All assays were conducted in 300 mM Tris-Citrate and 100 mM NaCl; ν= 10 mVs^{-1} for all the scans; The graph has been normalized in order to aid comparison.

For each voltammogram, the formal potential was also determined in order to possibly estimate a pKa value for the redox of the FDH (in this context pK_{ox} and pK_{red}). In figure 4.10, there is the beginning of a sigmoidal curve, but it was not possible to determine a pKa value. For that assays with pH values of 4, 4.5 and 8.5 should be performed. It is possible, however to see the tendency of the curve, to lower values of $E^{0'}$ with the pH increase, which is a typical behaviour of redox centres in enzymes due to an enhanced solvent exposition.[55]

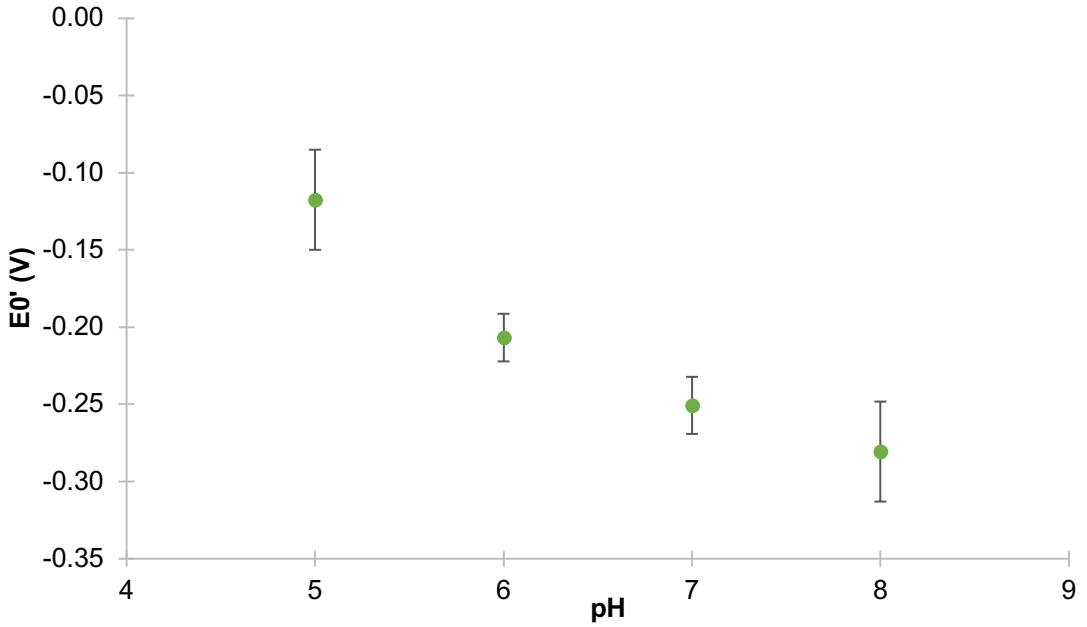

Figure 4.10 Dependence of the formal potential with pH

4.3 FDH Catalytic Characterisation towards CO_2 reduction

For the characterisation of the FDHs' catalysis with CO_2, three approaches were used: catalysis with the addition of sodium hydrogencarbonate, the addition of a saturated CO_2 solution and the addition of CO_2 in gaseous form directly inside the electrochemical cell's solution.

4.3.1 Catalysis with Sodium Hydrogencarbonate

In order to get a catalytic reaction, a solution of 0.47 mM sodium hydrogencarbonate was added to the electrolyte. When added to water, the sodium hydrogencarbonate is going to complete dissociate forming hydrogencarbonate. That hydrogencarbonate, in turn, is going to react with water forming carbonic acid. The acid also forms a hydration equilibrium with the water in which CO_2 is formed.

$$HCO_3^- + H_2O \rightleftharpoons H_2CO_3 + OH^- \qquad \text{Ka} = 4.47\text{x}10^{-7}\ (25\ ^\circ\text{C})[56] \qquad \text{Eq. 7}$$

$$H_2CO_3 \rightleftharpoons CO_2 + H_2O \qquad \text{Kh} = 1.7\text{x}10^{-3}\ (25\ ^{o})^{57} \qquad \text{Eq. 8}$$

In the figure 4.11, it is possible to observe and compare the differences in the cyclic voltammogram due to the catalysis processes of FDH.

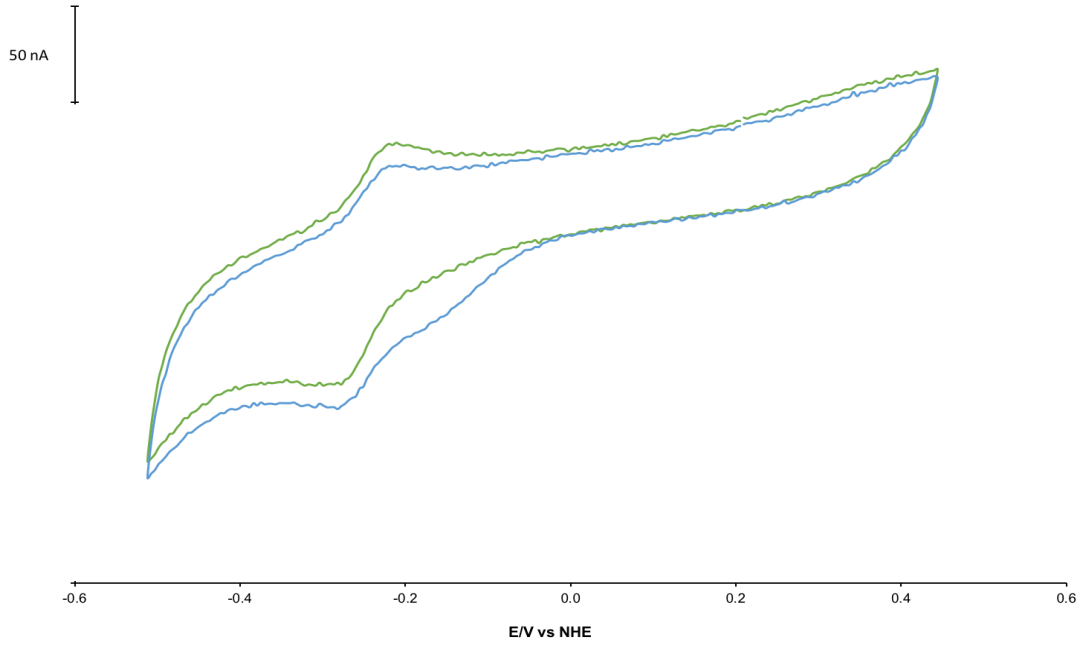

Figure 4.11 Cyclic voltammograms of FDH (7.9μm) before (green line) and after (blue line) of the addition of 0.47 mM sodium hydrogencarbonate. Both assays were performed in 300 mM Tris-HCl pH 7.5; 100 mM KNO_3 at v = 10 mVs^{-1}.

Comparing the two voltammograms, it is possible to see significant changes considering that both anodic and cathodic peak are affected and the appearance of a new one at -150 mV. In the cathodic peak, it is possible to see an increase in intensity of the signal while in the anodic peak, there is a decrease. These changes in the peaks during catalysis confirms that these are indeed the signals of the molybdenum atom in the active centre.

In order to confirm that the new signal was indeed due the catalysis with CO_2 and not with any other interference that could be present, a new assay was performed as control, replacing the solution of sodium hydrogencarbonate with the same added volume of water MilliQ. The results are seen in the figure 4.12.

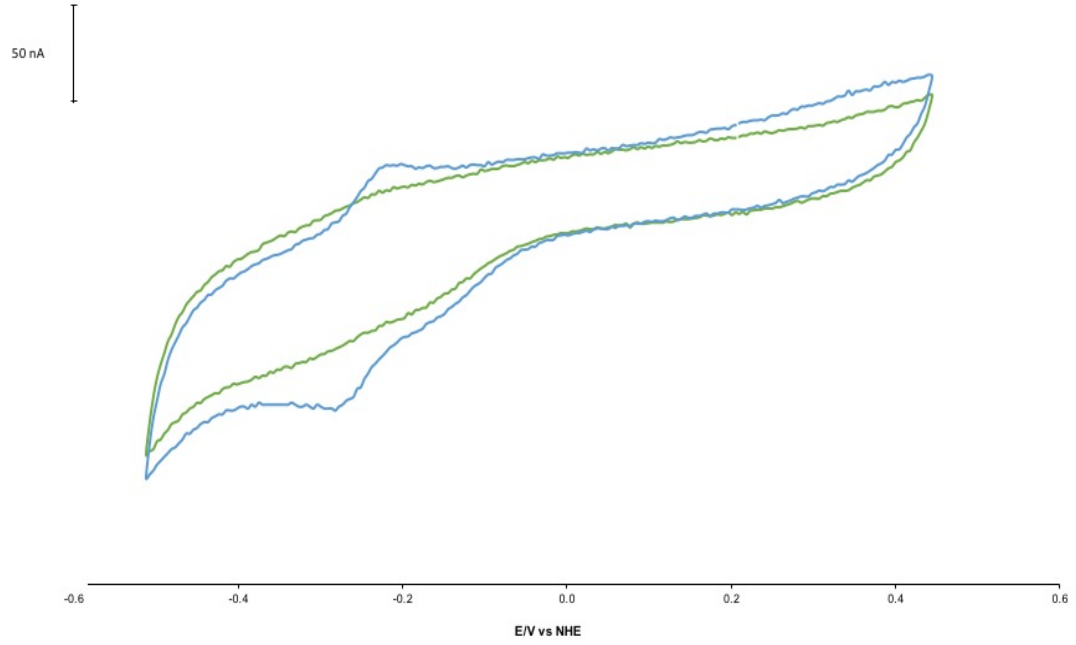

Figure 4.12 Cyclic voltammetry of FDH catalysis with sodium hydrogencarbonate (Blue line) and FDH water blank (green line) Both assays were performed in 300 mM Tris-HCl pH 7.5; 100 mM KNO_3 at v = 10 mVs^{-1}.

When analysisng the voltammogram of the assay performed with water, it is also possible to observe a peak present around the -150 mV. This indicated that the peak seen in the same potental in the sodium hydrogencarbonate voltammogram may not be due to the CO_2 catalytic reduction. Considering the potential of the peak, it sugests that an oxigenated species is present. These could be molecules of H_2O_2 that may be formed on the electrode surface due to the presence of some vestigial O_2.

4.3.2 Catalysis with a Saturate CO_2 solution

In order to obtain a higher concentration of CO_2 available for catalysis, a solution of MilliQ water was both degassed with Ar and saturated with gaseous CO_2 and then added into the electrolyte. Also, the scan rate was reduced from 10 mVs^{-1} to 2.5 mVs^{-1} to allow the diffusion of the CO_2 towards the electrode.

The concentration of the saturated CO_2 solution was calculated through Henry's Gas law. This states that the amount of gas dissolved in proportional to its partial pressure. Assuming that the partial pressure was 1 atm, the concentration of the solution added was 33.6 mM resulting in final concentration of 4.38 mM of CO_2 present in the assay.

As a result, the changes caused by the catalysis are much more defined, as it can be seen in the figure 4.13.

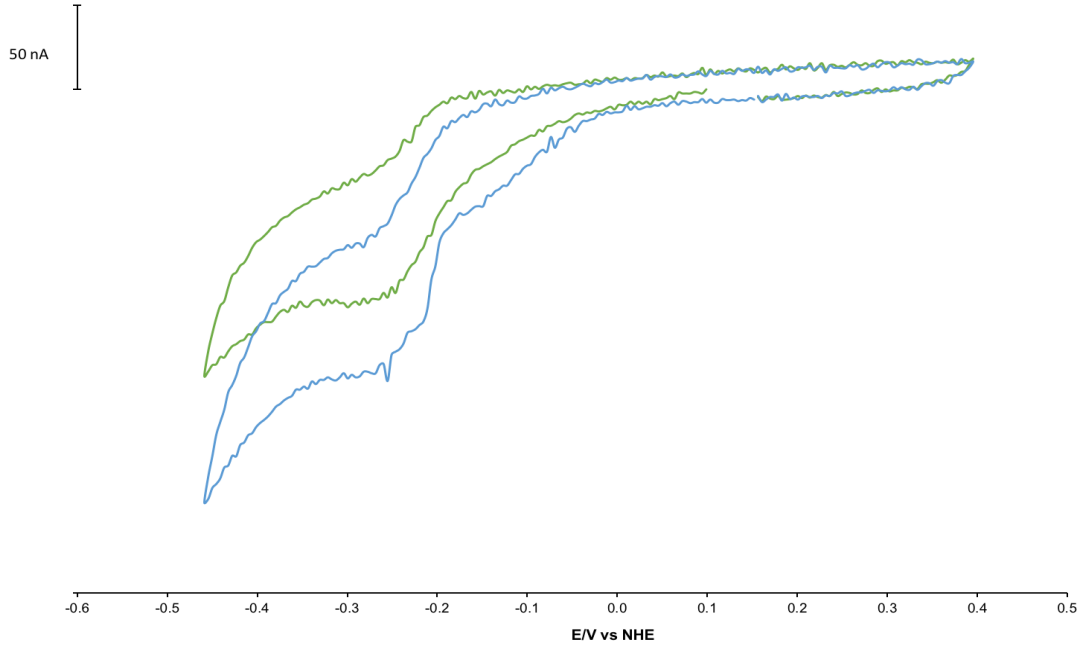

Figure 4.13 Cyclic voltammograms of FDH (7.9 μM) before (green line) and after (blue line) of the addition of 3 ml of 33.6 mM CO_2 saturated MilliQ water (final CO_2 concentration 4.38 mM); both assays were performed in 300 mM Tris-Citrate pH 7.5; 100 mM NaCl at v = 2.5 mVs^{-1}.

In this assay, both the cathodic peakes are much more well defined than in the previous seen with the addition of sodium bicarbnate. As last seen, the two cathodic peaks are increased when compared with the voltammogram without the saturated solution. The cathodic peak, present around -100 mV, is much better defined than previously. This second peak could be due the electronic transition state of the molybdenium atom from Mo(VI) to an intermediate state that is unstable, Mo(V), and rapidly decays into another state. The anodic peak, in this scan, also suffers a decrease in signal intensity, as it is seen in the assay done with sodium hydrogencarbonate.

In a multi scanning assay, it is possible to follow the steady decrease in the catalytic signal after the injection of the saturated solution. This can be seen in figure 4.14.

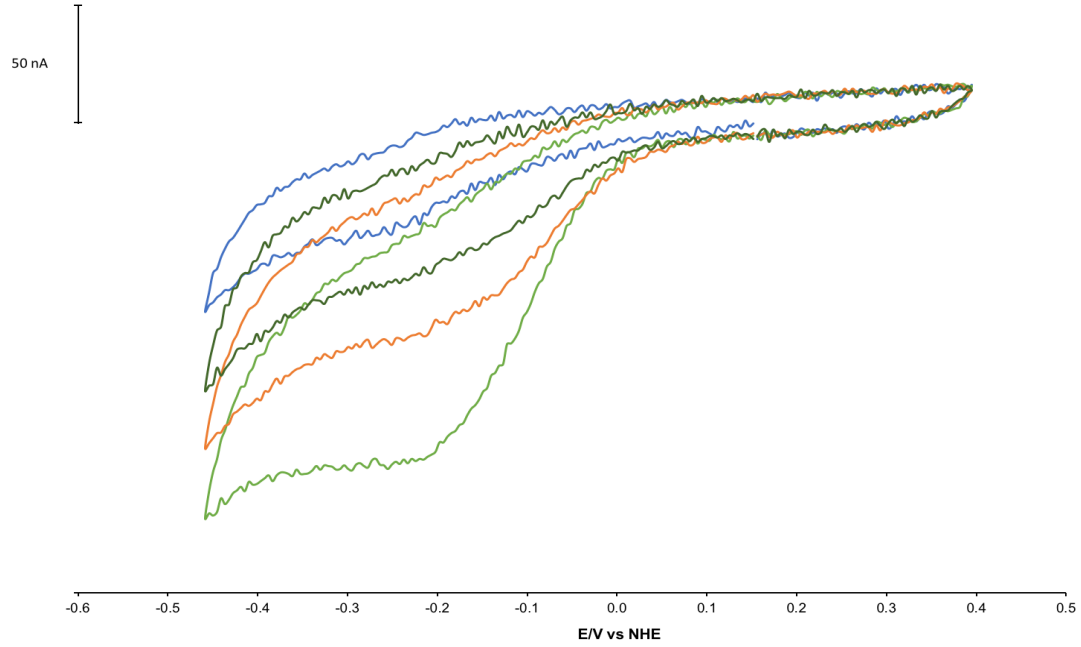

Figure 4.14 Evolution of the FDHs' signal after the adition of the 33.6 mM saturated solution of CO_2.. Final CO_2 concentration 4.38 mM; Blue line is the 1º scan; Light Green line is the 2º scan; Orange line is the 3º scan; Darker Green is the 4º Scan; All assays were performed in 300 mM Tris-Citrate pH 7.5; 100 mM NaCl at v = 2.5 mVs^{-1}.

During the first scan (blue line in figure 4.14) only the FDH' Mo centre redox signal is present considering that the saturated solution had not been added yet, thus allowing this scan to act as a baseline. During the first potentials around 200 mV of the second scan (Light Green line in figure 4.14), the 33.6 mM saturated CO_2 solution was added. During this scan it is possible to observe the CO_2 catalysis by the enhanced reduction current observed comparing with the 1st scan and the formation of a plateau, typical of a pseudo-steady state during catalysis. The maximum potential, in this turnover conditions, is around -200 mV. In following two scans (third corresponds to the Orange line and the fourth is the Darker Green line in figure 4.14), nothing else was added during this assay. So, during the 3º and 4º scan, as the substrate is consumed, it is possible to see a steady decrease of the signal, tending towards the first one, the only one without the substrate.

4.3.3. Catalysis with gaseous CO_2

In order to achieve a different and more direct way to introduce CO_2 in the solution, it was tested the direct introduction of CO_2 as gas. As so, 1 ml of CO_2 in gaseous (gCO_2) form was added to the electrolyte. Assuming that the pressure was 1 atm, the final concentration of CO_2 during the assay was 1.68 mM.

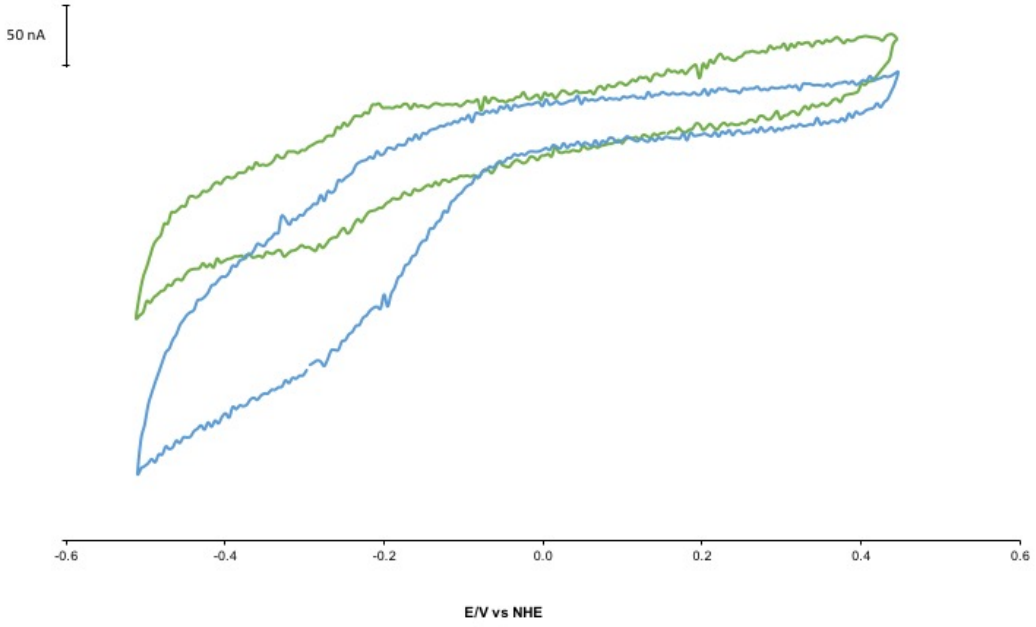

Figure 4.15 Cyclic voltammograms of FDH (7.9 μM) before (green line) and after (blue line) of the addition of 1 ml of gCO_2 for a final concentration of 1.68 mM Both assays were performed in 300 mM Tris-Citrate pH 7.5; 100 mM NaCl at v = 10 mVs^{-1}.

In figure 4.15, it is possible to see that the catalytic effects with gCO_2 are much better observed than the ones observed with sodium hydrogencarbonate and the addition using a saturated solution. In this assay, the cathodic peak has increase 1.1 times and the anodic peak is so diminished that is almost not seen. The cathodic peak is so pronounced that is impossible to ascertain if the new peak (around -100 mV) is also there but merged in the enhanced cathodic catalytic wave or not. Also, there is a decrease on the second anodic peak around 332 mV. This decrease in this peak during catalytic conditions could indicate that the peak belongs to other redox centres, like the Fe/S centres and/or haem *c* centres.

Again, in order to confirm that all the changes were due to the catalytic processes with the CO_2 and not for other species, other assay in non-turnover conditions was made but in these the addition of atmospheric air was performed.

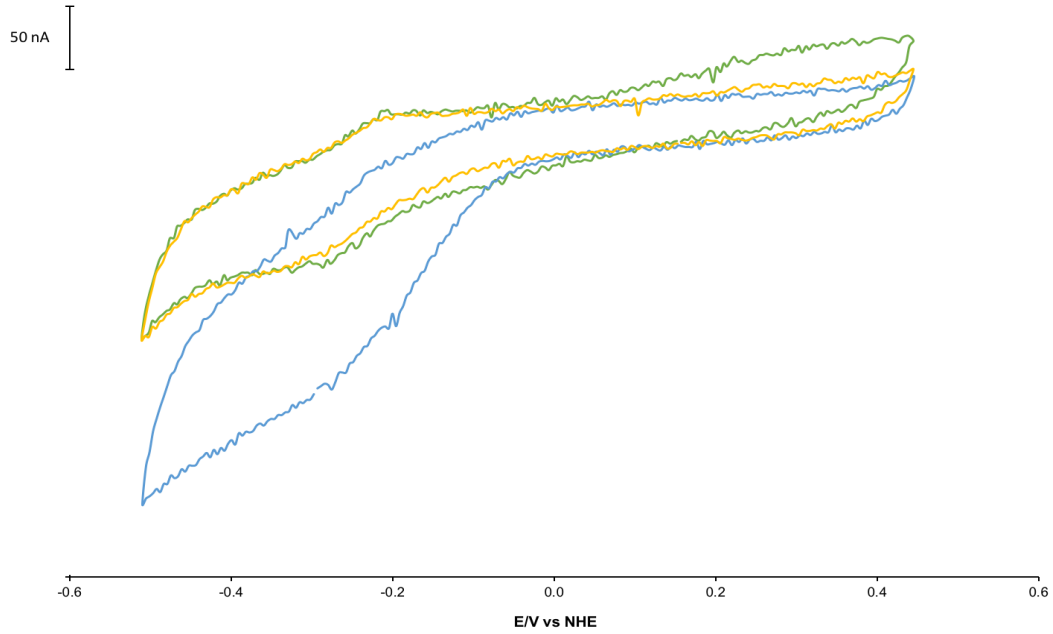

Figure 4.16 Cyclic voltammetry of FDH. The Green line represents simply FDH; The Blue line is FDH with the addition of 1ml of CO_2; The Yellow line is FDH with the addition of 1ml of atmospheric air. Both assays were performed in 300 mM Tris-citrate pH 7.5; 100 mM NaCl at v = 10 mVs^{-1}.

Analysing the voltammograms from figure 4.17, it is possible to see in the voltammogram where the atmospheric air was added (yellow curve), that there is no increase in the cathodic peak. This allows to conclude that the increase in the cathodic peak of the voltammogram with the addition of the CO_2 is indeed due to the catalysis and not due to the presence of other species, namely due to the presence of oxygen and its subsequent reduction. Also, when analysing the voltammogram when the atmospheric air was added, it seems that there is also a decrease in the second anodic peak around +332 mV as seen in the voltammogram with the addiction of the gCO_2. One explanation is that when adding atmospheric air, there is going to the addition of O_2 but also addition of the naturally present CO_2. Although the concentration of CO_2 added may be small, it could be enough to trigger some catalytic activity.

5. Conclusions and Future Remarks

In this work, the *D. desulfuricans* FDH was purified to a high degree of purity (120 times), with a very good recovery (17%).

The direct electrochemical response of a FDH was observed by cyclic voltammetry for the first time. The electrochemical characterisation of the *D. desulfuricans* FDH revealed a quasi-reversible system, with a redox pair with a formal potential of -245 $\pm$ 8 mV *vs* NHE, which was assigned to a redox process of the molybdenum atom in the enzyme active centre (transition Mo(VI)/Mo(IV)). Further assays in turnover conditions confirmed that the signal for this redox pair was due to the molybdenum centre catalytic current. A low k_{sh} for the redox pair, in non-turnover conditions, was obtained, indicating that this system has a slow electronic transfer rate. Concerning the characterisation of the FDH catalysis towards CO_2, all the three tested approaches were successful in obtaining a defined, consistent catalytic signal, with the best results being obtained with the addition of gaseous CO_2 .

In order to fully complete the FDHs electrochemical characterisation, further assays and the use of other techniques would be needed, such as:

- Completing the pH dependence of the Mo centre, in order to obtain a pKa of the molybdenum centre;
- Performing electrochemical assays using a rotating disk electrode to attain a steady-state allowing to calculate catalytic parameters, such a K_M;
- Perform assays with higher scan rates or other techniques (such as differential pulse voltammetry) to allow further study the other redox centres of the FDH enzyme.
- Perform assays in an anaerobic chamber to reduce the amount of air contamination.

6. References

1 S. Shafiee and E. Topal, *Energy Policy*, 2009, **37**, 181–189.

2 A. M. Appel, J. E. Bercaw, A. B. Bocarsly, H. Dobbek, D. L. DuBois, M. Dupuis, J. G. Ferry, E. Fujita, R. Hille and P. J. A. Kenis, *Chem. Rev.*, 2013, **113**, 6621–6658.

3 D. A. Lashof and D. R. Ahuja, *Nature*, 1990, **344**, 529–531.

4 K. Caldeira and M. E. Wickett, *Nature*, 2003, **425**, 365.

5 S. C. Doney, V. J. Fabry, R. A. Feely and J. A. Kleypas, *Annu. Rev. Mar. Sci.*, 2009, **1**, 169–192.

6 A. Alissandratos and C. J. Easton, *Beilstein J. Org. Chem.*, 2015, **11**, 2370.

7 M. Z. Jacobson, *Energy Environ. Sci.*, 2009, **2**, 148–173.

8 C. Rice, S. Ha, R. I. Masel, P. Waszczuk, A. Wieckowski and T. Barnard, *J. Power Sources*, 2002, **111**, 83–89.

9 S. Ha, Z. Dunbar and R. I. Masel, *J. Power Sources*, 2006, **158**, 129–136.

10 Y. i Hori, in *Modern aspects of electrochemistry*, Springer, 2008, pp. 89–189.

11 S. Grimaldi, B. Schoepp-Cothenet, P. Ceccaldi, B. Guigliarelli and A. Magalon, *Biochim. Biophys. Acta - Bioenerg.*, 2013, **1827**, 1048–1085.

12 T. Hartmann, N. Schwanhold and S. Leimkühler, *Biochim. Biophys. Acta - Proteins Proteomics*, 2015, **1854**, 1090–1100.

13 L. B. Maia, I. Moura and J. J. G. Moura, *Inorganica Chim. Acta*, 2017, **455**, 350–363.

14 M. Leopoldini, N. Russo, M. Toscano, M. Dulak and T. A. Wesolowski, *Chem. Eur. J.*, 2006, **12**, 2532–2541.

15 G. Unden and J. Bongaerts, *Biochim. Biophys. Acta - Bioenerg.*, 1997, 1320, 217–234.

16 P. J. Gonzalez, M. G. Rivas, C. S. Mota, C. D. Brondino, I. Moura and J. J. G. Moura, *Coord. Chem. Rev.*, 2013, **257**, 315–331.

17 J. R. Andreesen, E. El Ghazzawi and G. Gottschalk, *Arch. Microbiol.*, 1974, **96**, 103–118.

18 U. RUSCHING, U. MULLER, P. WILLNOW and T. HOPNER, *Eur. J. Biochem.*, 1976, **70**, 325–330.

19 A. Sigel and H. Sigel, *Metals Ions in Biological System: Volume 39: Molybdenum and Tungsten: Their Roles in Biological Processes:*, Taylor & Francis, 2002.

20 I. G. Shabalin, E. V. Filippova, K. M. Polyakov, E. G. Sadykhov, T. N. Safonova, T. V.

Tikhonova, V. I. Tishkov and V. O. Popov, *Acta Crystallogr. Sect. D Biol. Crystallogr.*, 2009, **65**, 1315–1325.

21 a a Alekseeva, S. S. Savin and V. I. Tishkov, *Acta Naturae*, 2011, **3**, 38–54.

22 L. B. Maia, J. J. G. Moura and I. Moura, *J. Biol. Inorg. Chem.*, 2015, **20**, 287–309.

23 J. C. Boyington, V. N. Gladyshev, S. V Khangulov, T. C. Stadtman and P. D. Sun†, *Science (80-.).*, 1997, **275**, 1305.

24 V. N. Gladyshev, J. C. Boyington, S. V. Khangulov, D. A. Grahame, T. C. Stadtman and P. D. Sun, *J. Biol. Chem.*, 1996, **271**, 8095–8100.

25 M. Jormakka, B. Byrne and S. Iwata, *Curr. Opin. Struct. Biol.*, 2003, **13**, 418–423.

26 M. J. Almendra, C. D. Brondino, O. Gavel, A. S. Pereira, P. Tavares, S. Bursakov, R. Duarte, J. Caldeira, J. J. G. Moura and I. Moura, *Biochemistry*, 1999, **38**, 16366–16372.

27 H. Raaijmakers, S. Macieira, J. M. Dias, S. Teixeira, S. Bursakov, R. Huber, J. J. Moura, I. Moura and M. J. Romao, *Structure*, 2002, **10**, 1261–1272.

28 C. S. Mota, M. G. Rivas, C. D. Brondino, I. Moura, J. J. G. Moura, P. J. González and N. M. F. S. A. Cerqueira, *J. Biol. Inorg. Chem.*, 2011, **16**, 1255–1268.

29 H. C. A. Raaijmakers and M. J. Romão, *JBIC J. Biol. Inorg. Chem.*, 2006, **11**, 849–854.

30 P. M. Matias, I. A. C. Pereira, C. M. Soares and M. A. Carrondo, *Prog. Biophys. Mol. Biol.*, 2005, **89**, 292–329.

31 I. A. C. Pereira, A. R. Ramos, F. Grein, M. C. Marques, S. M. da Silva and S. S. Venceslau, *Front. Microbiol.*, 2011, **2**.

32 C. Costa, M. Teixeira, J. LeGall, J. J. G. Moura and I. Moura, *J. Biol. Inorg. Chem.*, 1997, **2**, 198–208.

33 M. G. Rivas, P. J. González, C. D. Brondino, J. J. G. Moura and I. Moura, *J. Inorg. Biochem.*, 2007, **101**, 1617–1622.

34 L. B. Maia, L. Fonseca, I. Moura and J. J. G. Moura, *J. Am. Chem. Soc.*, 2016, **138**, 8834–8846.

35 R. K. THAUER, B. KÄUFER and G. FUCHS, *FEBS J.*, 1975, **55**, 111–117.

36 E. V Filippova, K. M. Polyakov, T. V Tikhonova, T. N. Stekhanova, K. M. Boiko and V. O. Popov, *Crystallogr. Reports*, 2005, **50**, 796–800.

37 P. N. Bartlett, *Bioelectrochemistry: Fundamentals, Experimental Techniques and Applications*, Wiley, 2008.

38 C. Banks, R. Mortimer and S. McIntosh, *Electrochemistry*, The Royal Society of Chemistry, 2016, vol. 13.

39 C. M. A. Brett and A. M. O. Brett, *Electrochemistry: Principles, Methods, and Applications*, Oxford University Press, 1993.

40 D. F. Yancey, E. V Carino and R. M. Crooks, *J. Am. Chem. Soc.*, 2010, **132**, 10988–10989.

41 R. M. Crooks and M. Zhao, *Adv. Mater.*, 1999, **11**, 217–220.

42 G. L. M. Santa, S. M. S. A. Bernardino, S. Magalhães, V. Mendes, M. P. C. Marques, L. P. Fonseca and P. Fernandes, *Appl. Biochem. Biotechnol.*, 2011, **165**, 1–12.

43 N. S. Spinner, J. A. Vega and W. E. Mustain, *Catal. Sci. Technol.*, 2012, **2**, 19–28.

44 D. T. Whipple and P. J. A. Kenis, *J. Phys. Chem. Lett.*, 2010, **1**, 3451–3458.

45 C. A. Cotton, C. Edlich-Muth and A. Bar-Even, *Curr. Opin. Biotechnol.*, 2018, **49**, 49–56.

46 C. Mourato, M. Martins, S. M. da Silva and I. A. C. Pereira, *Bioresour. Technol.*, 2017, **235**, 149–156.

47 K. Sakai, B. C. Hsieh, A. Maruyama, Y. Kitazumi, O. Shirai and K. Kano, *Sens. Bio-Sensing Res.*, 2015, **5**, 90–96.

48 K. Sakai, Y. Kitazumi, O. Shirai and K. Kano, *Electrochem. commun.*, 2016, **65**, 31–34.

49 T. Reda, C. M. Plugge, N. J. Abram and J. Hirst, *Proc. Natl. Acad. Sci.*, 2008, **105**, 10654–10658.

50 A. Bassegoda, C. Madden, D. W. Wakerley, E. Reisner and J. Hirst, *J. Am. Chem. Soc.*, 2014, **136**, 15473–15476.

51 I. Moura, L. B. Maia, S. R. Pauleta and J. J. G. Moura, 2016.

52 U. K. LAEMMLI, *Nature*, 1970, **227**, 680.

53 W. E. Robinson, A. Bassegoda, E. Reisner and J. Hirst, *J. Am. Chem. Soc.*, 2017.

54 E. Laviron, *J. Electroanal. Chem.*, 1979, **101**, 19–28.

55 T. C. Santos, A. R. De Oliveira, J. M. Dantas, C. A. Salgueiro and C. M. Cordas, *Biochim. Biophys. Acta - Bioenerg.*, 2015, **1847**, 1113–1118.

56 N. N. Greenwood and A. Earnshaw, *Chemistry of the Elements*, Elsevier Science, 2012.

57 C. E. Housecroft and A. G. Sharpe, *Inorganic Chemistry*, Pearson Prentice Hall, 2nd Ed., 2005.

58 J. Jouzel, V. Masson-Delmotte, O. Cattani, G. Dreyfus, S. Falourd, G. Hoffmann, B. Minster, J. Nouet, J. M. Barnola and J. Chappellaz, *IGBP PAGES/World Data Cent. Paleoclimatology data Contrib. Ser.*, 2007, **91**, 2007.

Appendix

Appendix A - Electrochemical criteria for thin layer electrochemical systems

The thin layer theory is applied when both electroactive species, oxidized and reduced, are constricted within a thin layer on the surface of the electrode. If this layer is smaller than the diffusion layer, then the diffusion parameters can be disregarded.

The reversibility criteria for this system are:

- I_p a v, the current peak varies with the scan rate
- ΔEp α v, there is no separation between the anodic and the cathodic current peaks
- The curve is symmetrical around E_p
- $I_{pa}/I_{pa} \approx 1$

The peak current for a reversible reaction is given by:

$$I_p = \frac{n^2 F^2 \nu V [O]_i}{4RT}$$

Appendix B - Laviron's mathematical approach

The use of a thin layer allows for the use of Laviron's mathematical approach for diffusional electrochemical systems to determine kinetic parameters. Laviron derived general expressions for the linear potential sweep voltammetric response in thin layer voltammetry when both the oxidized and the reduced forms are strongly adsorbed.

A parameter *m* is defined by the following equation:

$$m = \frac{RTk_{sh}}{Fnv}$$

From the experimental difference between the peak potential of the anodic and the cathodic peaks, ΔE_p, and for a known α, the k_{sh} can be calculated. Two cases can be considered,

1. $\Delta E_p > 200/n$ and

2. $\Delta E_p < 200/n$ mV.

For case 1., the α can be calculated by the plot of E_p vs. log v, with slopes equal to -2.3RT/αnF and 2.3RT/(1-α)nF for the cathodic and anodic peaks, respectively. From it is possible to calculate k_{sh} from the equation:

$$k_{sh} = \frac{\alpha \mathrm{nFv}}{RT} = \frac{(1 - \alpha n F v_a)}{RT}$$

For case 2., the determination of α cannot be precise, but for values close to 0.5 (between 0.3 and 0.7), the k_{sh} can still be determined with a negligible error. From a theoretical curve of $n\Delta E_p$ as a function of 1/*m*, and from interpolation of the experimental ΔE_p values, the m parameter can be found and, so, using equation B.8, the k_{sh} is estimated.

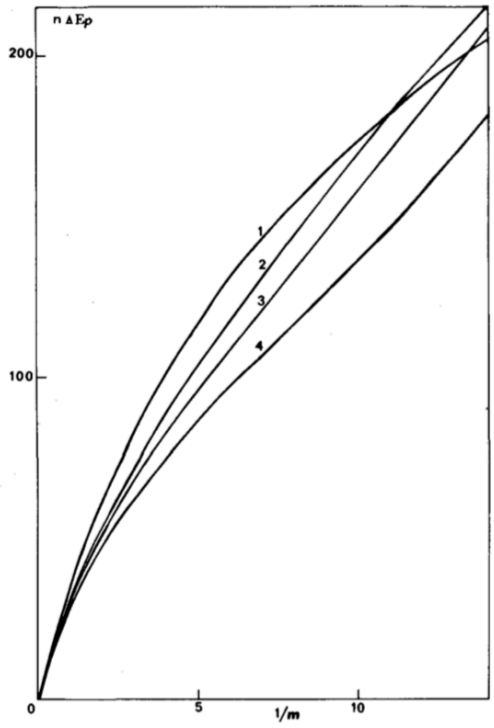

Figure B.1 Variations of with 1/m. (1) α = 0.5, (2) α = 0.8, (3) α = 0.85 (4) α = 0.9

Appendix C - Protein Quantification

In order to quantify the total concentration of protein in the samples, a modified version of the Lowry/Biuret method was used. In this modified method, 0.4mL of Biuret reagent was added to 0,1mL of sample. The Biuret reagent contains 0.15 % of hydrated cupper sulphite, 0.6% of potassium sodium tartrate, 3% of sodium hydroxide and 0.1% of potassium iodine.

After a 10 minute period of incubation, 3.5 mL of a 2.3% sodium carbonate and 0.1mL of Folin-Ciocalteu's phenol reagent was added. The solution was mixed in a vortex and incubated once more, this time for 30 minutes. Finally, the absorbance was measured at 750 nm.